Journal of Archaeological Science: Reports 71 (2026) 105608

Contents lists available at ScienceDirect

Journal of Archaeological Science: Reports

journal homepage: www.elsevier.com/locate/jasrep

Archaeometric characterization of Early Bronze Age building materials in the Iberian Peninsula. An example from Central Spain, the Bocapucheros site (Almagro, Ciudad Real)

Ángel De La Rosa Velasco [a], Luis Benítez de Lugo Enrich [b,*], Alfredo Mederos Martín [c], Jesús Rodríguez Pérez [a], Gonzalo Ruiz [d], Rodrigo Moreno [e]

[a] DIMME, Grupo de Durabilidad e Integridad Mecánica de Materiales Estructurales, Universidad Rey Juan Carlos, C. Tulipán s/n, 28933 Móstoles, Madrid, Spain
[b] Dpto. de Prehistoria, Historia Antigua y Arqueología, Facultad de Geografía e Historia, Universidad Complutense de Madrid, Edif. Filosofía B, C. Profesor Aranguren s/n, 28040 Madrid, Spain
[c] Dpto. de Prehistoria y Arqueología, Facultad de Filosofía y Letras, Universidad Autónoma de Madrid, Campus de Cantoblanco, 28049 Madrid, Spain
[d] ETSI Caminos, C. y P., Universidad de Castilla-La Mancha, Av. Camilo José Cela 2, 13071 Ciudad Real, Spain
[e] Instituto de Cerámica y Vidrio (CSIC), C. Kelsen 5, Campus de Cantoblanco, 28049 Madrid, Spain

ARTICLE INFO

Keywords:
Bronze Age buildings
Stone masonry
Earth mortars
Material characterization
Structural durability
Heritage conservation
14 C

ABSTRACT

This study provides a thorough characterization of the stone and earth-based construction materials from the Bronze Age funerary site of Bocapucheros (Almagro, Spain), emphasizing their composition, structural roles, absolute dating (14 C) and degradation processes. The load-bearing system consists exclusively of masonry walls built with locally sourced quartzitic blocks, shaped and assembled using manual techniques. Structural elements, including lintels and corbelled vaults, display different types of fracture modes caused by long-term mechanical and environmental stresses. Despite these damages, the overall stability is preserved thanks to a robust design that effectively distributes compressive loads.

A multi-phase construction sequence is proposed, encompassing site preparation, foundation laying, wall assembly, and corbelled pseudo-dome roofing. The mortars are earth-based, primarily composed of aluminosilicate clays such as muscovite and kaolinite, combined with varying proportions of quartz aggregates, alongside traces of carbonates and iron oxides. Analyses performed using radiocarbon dating, X-ray diffraction, Fourier-transform infrared spectroscopy, Raman spectroscopy, X-ray fluorescence, and backscattered electron microscopy coupled with energy-dispersive X-ray spectroscopy confirm the compositional diversity and the presence of volcanic and metamorphic components consistent with the local geological context. Thermogravimetric and calorimetric data reveal dehydration and decarbonation processes aligned with the behavior of clay minerals and carbonates. This integration of mechanical resilience, material heterogeneity, and advanced corbelling techniques reflects sophisticated architectural knowledge within Bronze Age society. These findings advance the understanding of prehistoric construction technologies and support ongoing efforts in cultural heritage preservation.

1. Introduction

Earth has played a fundamental role in the history of construction, serving as one of the earliest and most widely used building materials. Since ancient times, humans have utilized naturally available resources such as stone, wood, and earth—either in their raw state or subjected to varying degrees of processing. These materials were combined using construction techniques that varied in complexity, from relatively simple or rudimentary methods to carefully executed approaches, resulting in structural forms specifically adapted to both functional requirements and environmental conditions (Gómez Morgade et al., 2021).

Earthen mortars have been used since the Neolithic period as both binding agents and protective coatings for stone or earthen architecture (Gómez Morgade et al., 2021; Pastor Quiles, 2017; Jover Maestre et al., 2016). These mortars often included lime and organic additives,

* Corresponding author.
E-mail addresses: luisbeni@ucm.es (L. Benítez de Lugo Enrich), alfredo.mederos@uam.es (A. Mederos Martín).

https://doi.org/10.1016/j.jasrep.2026.105608
Received 21 December 2025; Accepted 25 January 2026
Available online 25 February 2026

Fig. 1. La Encantada settlement, Bronze Age (Granátula de Calatrava, Ciudad Real, Spain): (a) general view of the walled settlement (Sánchez Meseguer et al., 2019); (b) view from the upper part of the site (Estudio Arqueología, 2025); (c) detail of quartzitic stone masonry sourced from the surrounding mountain range (Estudio Arqueología, 2025).

enhancing their performance (Pastor Quiles, 2017; Jover Maestre et al., 2016). Despite the increasing use of stone during the Bronze Age, earth remained indispensable, especially in foundations and masonry mortars. Frequently, stone walls were erected atop dry-laid or earthen-mortar-bound foundations, while other structural components continued to employ traditional earth-based techniques (Gómez Morgade et al., 2021).

By the second millennium BC, monumental architecture, particularly associated with funerary practices, demonstrated advanced technical skills and deliberate spatial organization. These constructions—requiring considerable labor and planning—reflected both engineering knowledge and social symbolism (García Amengual, 2006). Site selection was based on symbolic and functional considerations, including topographic prominence, visibility, access to raw materials and proximity to existing settlements. Stone was commonly used as the primary construction material, obtained from nearby sources (García Amengual, 2006).

The structural complexity observed in Bronze Age funerary sites of the Iberian Peninsula suggests prior architectural planning and emerging sociopolitical organization. These characteristics, previously identified in Copper Age contexts, point to the existence of early hierarchical societies, where access to resources and labor was unequally distributed (Díaz del Río Español, 2004). Monumental architecture thus represents a valuable archaeological indicator of power structures and collective identity. The use of cyclopean masonry—comprising large stone blocks laid dry or bonded with earthen mortar—was the predominant construction technique. Foundations were established on bedrock or stone socles, with initial courses stabilized using wedges and subsequent stones laid horizontally. Earth ramps or basic pulley systems facilitated vertical construction (García Amengual, 2006).

Despite the prominence of stone, earthen materials remained integral due to their accessibility, versatility, and adaptability. Since the Neolithic, earth mortars were widely used in the southwestern Iberian Peninsula, initially to coat pits and later, during the Copper and Bronze Ages, as binders in stone masonry, mudbrick construction, and coverings or fillings in vegetal structures, as well as likely in solid walls (Bruno and Faria, 2008). Studies of prehistoric sites in southern Portugal document diverse techniques—clay renders, mortars with branch imprints, handmade or moulded mudbricks, and stacked-earth walls—preserved by fire and providing key insights for technological reconstructions (Bruno et al., 2010). Notable examples include La Encantada (Ciudad Real, Spain) (Fig. 1), with large quartzite blocks bonded with mortar (Sánchez Meseguer et al., 2004), and Cabezo Pardo (Alicante, Spain), where El Argar settlements likely employed earth mortars (Pastor Quiles, 2017) or clay-lime mortars in walls and floors at La Almoloya (Murcia, Spain) (Lull et al., 2021). In Los Llanetes (Huelva, Spain), monuments were constructed with stones bonded using clay mortars (Linares-Catela et al., 2023), while at Castro de Santa Trega (Pontevedra, Spain), Iron Age walls reveal exclusive use of local earth mortars and plasters (Gómez Morgade et al., 2021). Small collective Copper Age tombs, such as La

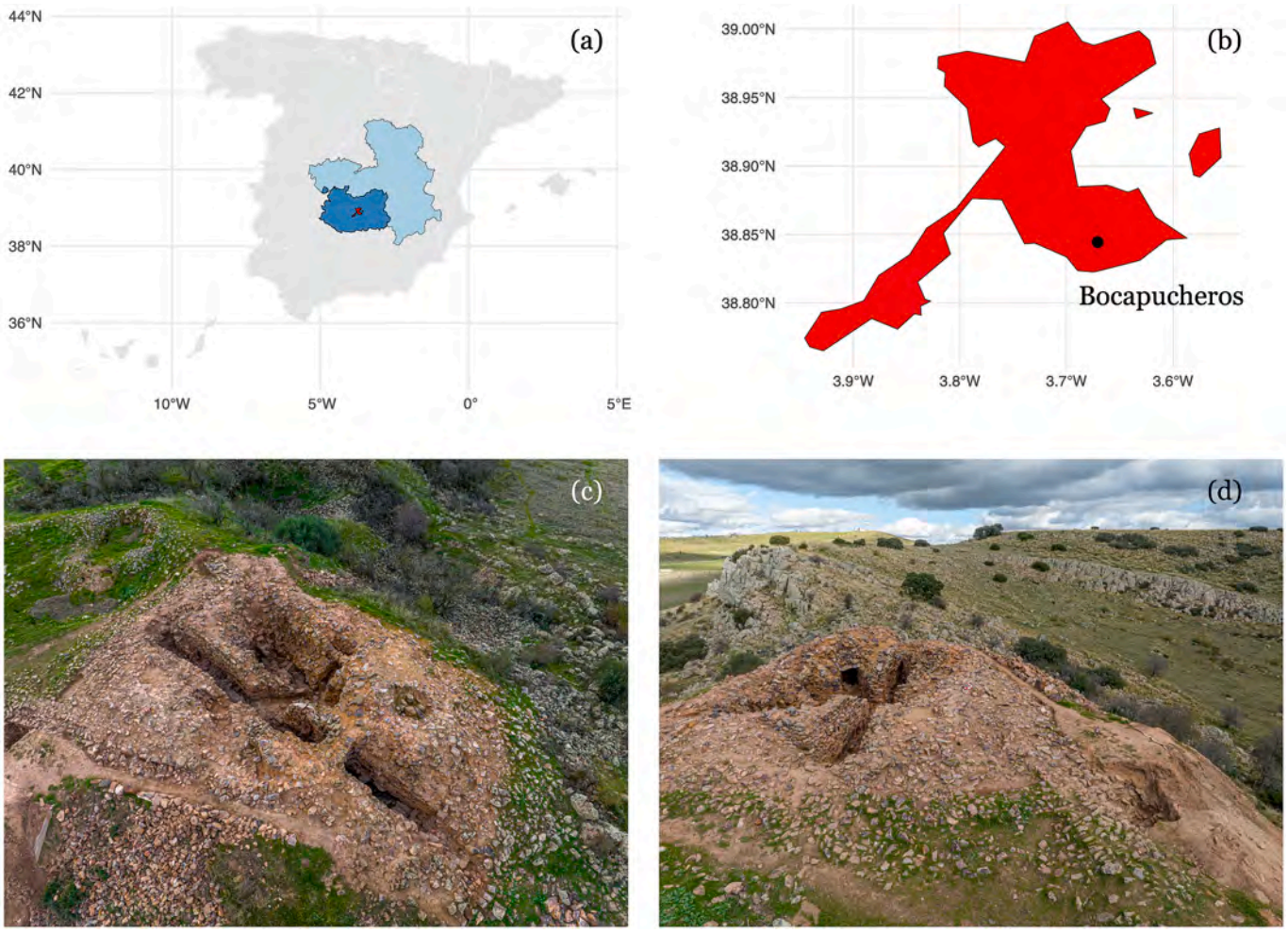

Fig. 2. Bocapucheros funerary complex (19–17 th centuries BC): (a) location on the map of Spain (source: mapSpain); (b) location within the municipality of Almagro (source: mapSpain); (c) aerial view of the monumental complex (source: Bocapucheros Project); (d) aerial view of the complex and the surrounding quartzitic hills in the southern volcanic sector of Campo de Calatrava, Spain (source: Bocapucheros Project).

Table 1
Radiocarbon and isotopic analysis of two human individuals buried in Bocapucheros.

Id	Material	Radiocarbon lab code	^{14}C BP	Cal BC (1σ)	Cal BC (2σ)	δ^{13}C (‰)	δ^{15}N (‰)	%C	%N	C:N
BP-1	Human phalanx	Beta-574064	3470 ± 30	1876–1703	1884–1692	−18.8	11.04	42.95	15.68	3.2
BP-2	Human jaw	Beta-604904	3440 ± 30	1871–1689	1878–1632	−18.4	9.26	37.45	13.35	3.3

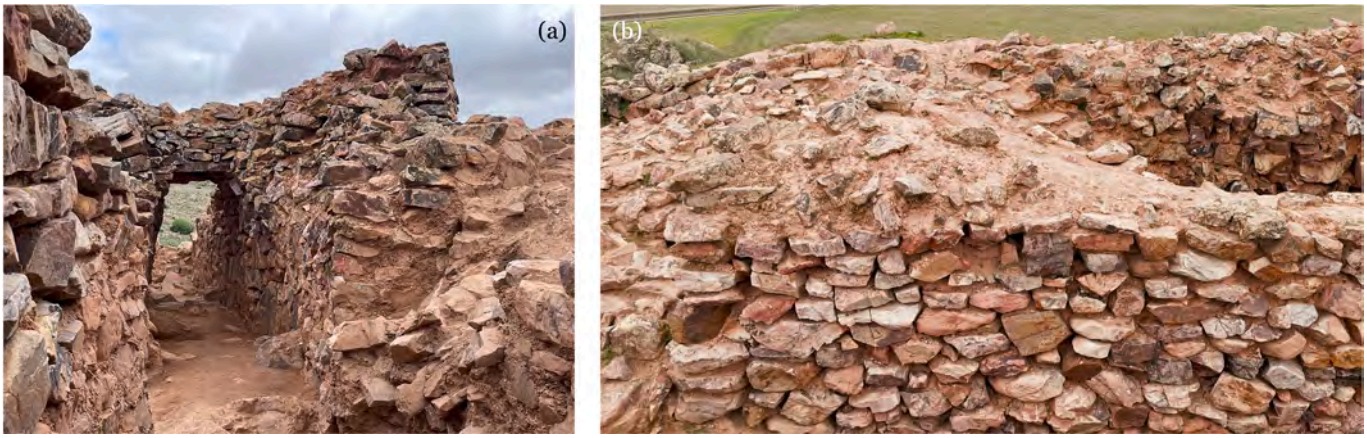

Fig. 3. Masonry of the monumental complex constructed with quartzite stone blocks of varying sizes: (a) detail of corridor wall; (b) detail of chamber walls.

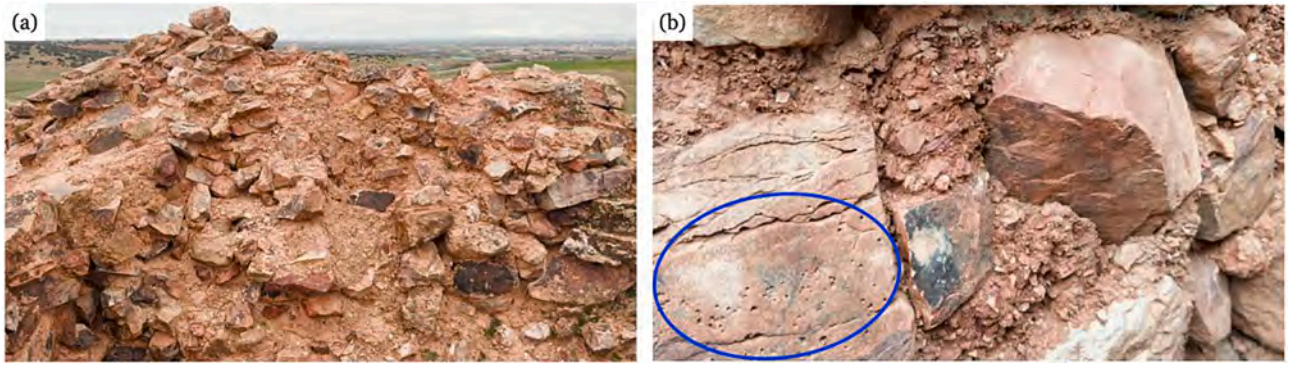

Fig. 4. Representative sampling of earth-based mortars from selected masonry joints in the monument: (a) upper section of the tumulus; (b) earth mortar or earthen concrete used as a bonding material within the masonry (detail showing tool marks on worked stone surfaces, highlighted within the blue oval).

Fig. 5. Monumental spatial design: (a) large lintel with oversized cross-sections in a corridor; (b) large lintel with oversized cross-sections and heavy covering at the entrance of a chamber.

Orden-Seminario (Huelva), also utilized mud and clay mortars (Linares-Catela and Vera-Rodríguez, 2023). Collectively, these cases illustrate the widespread and versatile use of earth mortars in prehistoric contexts across the Iberian Peninsula (Pastor Quiles, 2021). Typical formulations included soil and water, often modified with plant fibers or organic additives such as dung, animal fats, or even human remains, which enhanced mechanical performance and durability (Gómez Morgade et al., 2021; Pastor Quiles, 2017; Jover Maestre et al., 2016). Techniques such as wattle-and-daub or hand-molded earth persisted until more standardized earthen wall construction methods became widespread (Gómez Morgade et al., 2021).

During Late Prehistory, the production and use of lime as a binder constituted a major technological innovation, applied in mortars, floor and wall coatings, and decorative finishes to enhance durability and mechanical performance (Pastor Quiles, 2017; Jover Maestre et al., 2016). Lime and gypsum were among the first materials intentionally modified through chemical processes, representing a significant step in prehistoric material technology (Brysbaert, 2007; Jover Maestre et al., 2016; Pastor Quiles, 2021; Hobbs and Siddall, 2011). In the Iberian Peninsula, lime use may have begun as early as the late 3rd millennium BC, particularly in the Levantine region, and became more selective during the 2nd millennium BC, reflecting differences in structural function and social importance (Jover Maestre et al., 2016; Pastor Quiles, 2021; Garfinkel, 1987). Contrary to earlier hypotheses suggesting the

Fig. 6. Different fracture modes observed in the monumental complex: (a) detail showing an interior lintel fractured in mode I at the entrance to a chamber; (b) detail of a mixed-mode open fracture inside one of the chambers; (c) detail of a mixed-mode open fracture on one of the corridor lintels.

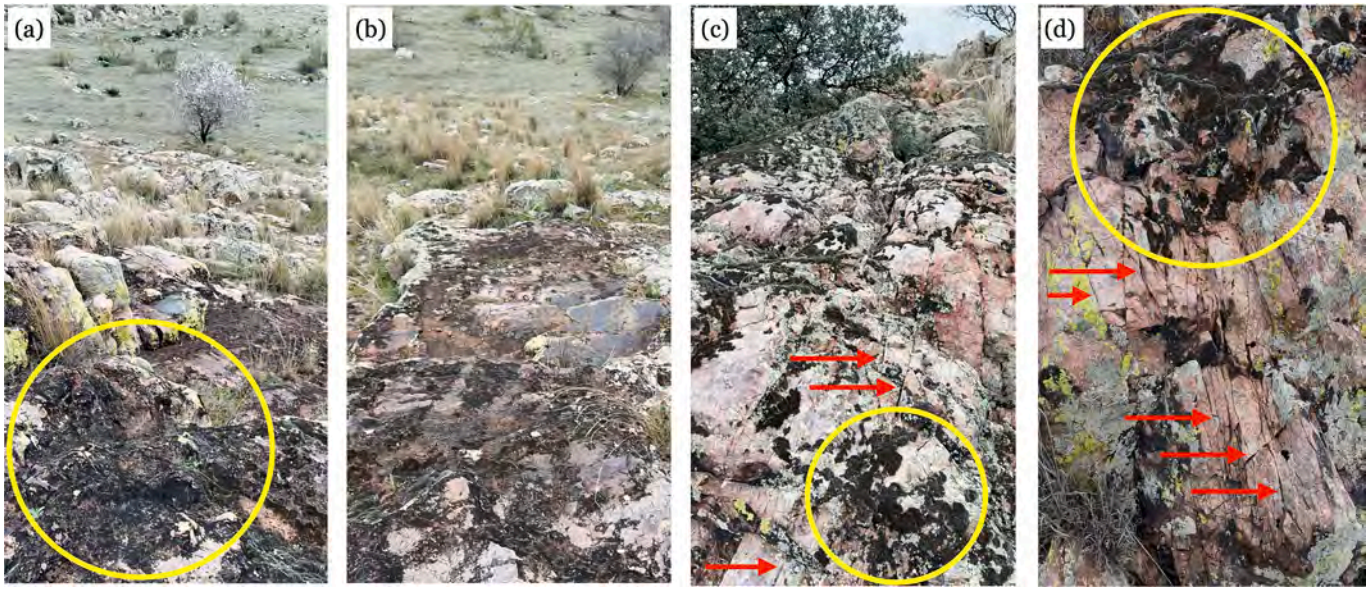

Fig. 7. Location of Stone Resources: (a, b) quarry site located near the construction area, exploited for stone extraction; (c) tool marks (red arrows) indicating controlled fracturing techniques used to detach stone blocks; (d) close-up view of tool marks (red arrows) related to the same fracturing process. In all images, black-colored lichen colonization (yellow circle) is visible on soil residues left behind after the removal of rock fragments.

use of lime or advanced treatments in Bronze Age mortars (Rodríguez, 2018), recent analyses at sites such as Castro de Santa Trega indicate that local saprolitic soils were used without lime addition, highlighting a practical approach based on material availability (Gómez Morgade et al., 2021; De la Peña, 1992). For instance, at the Argaric Bronze Age site of La Almoloya (Murcia, southeastern Spain), stone walls and floors in specific rooms were coated with clay-and-lime mortars, illustrating a clear technological advance (Lull et al., 2021). These examples underscore the uneven spatial and temporal distribution of lime technology across the Iberian Peninsula and highlight the interplay between

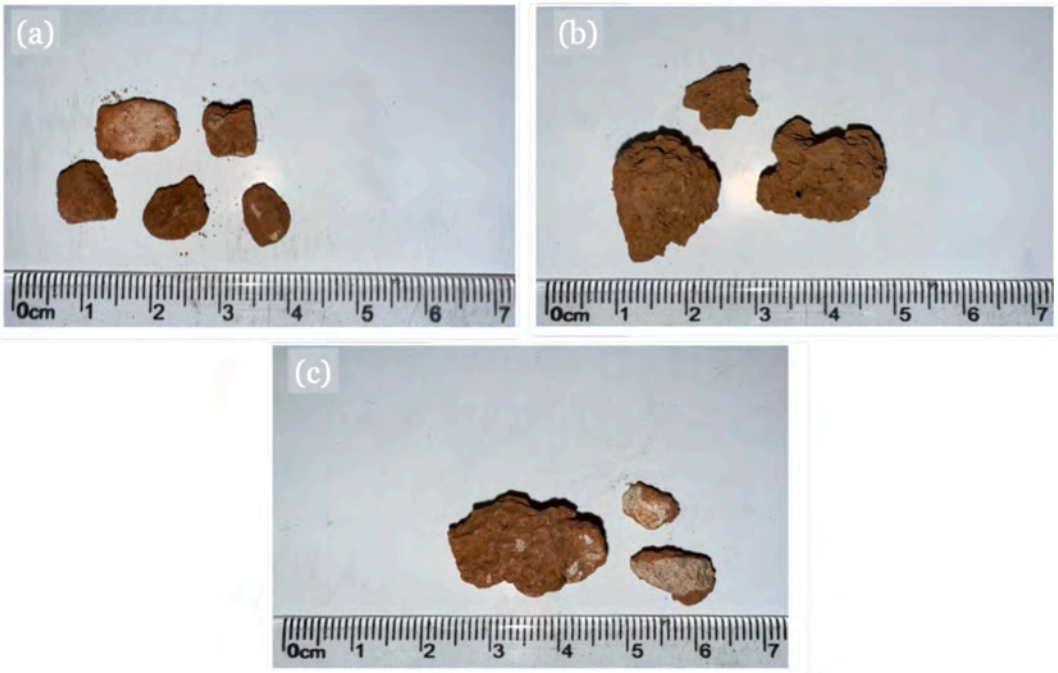

Fig. 8. Samples of earth mortar extracted for analysis: (a) BP-25-2, (b) BP-25-3, and (c) BP-25-5.

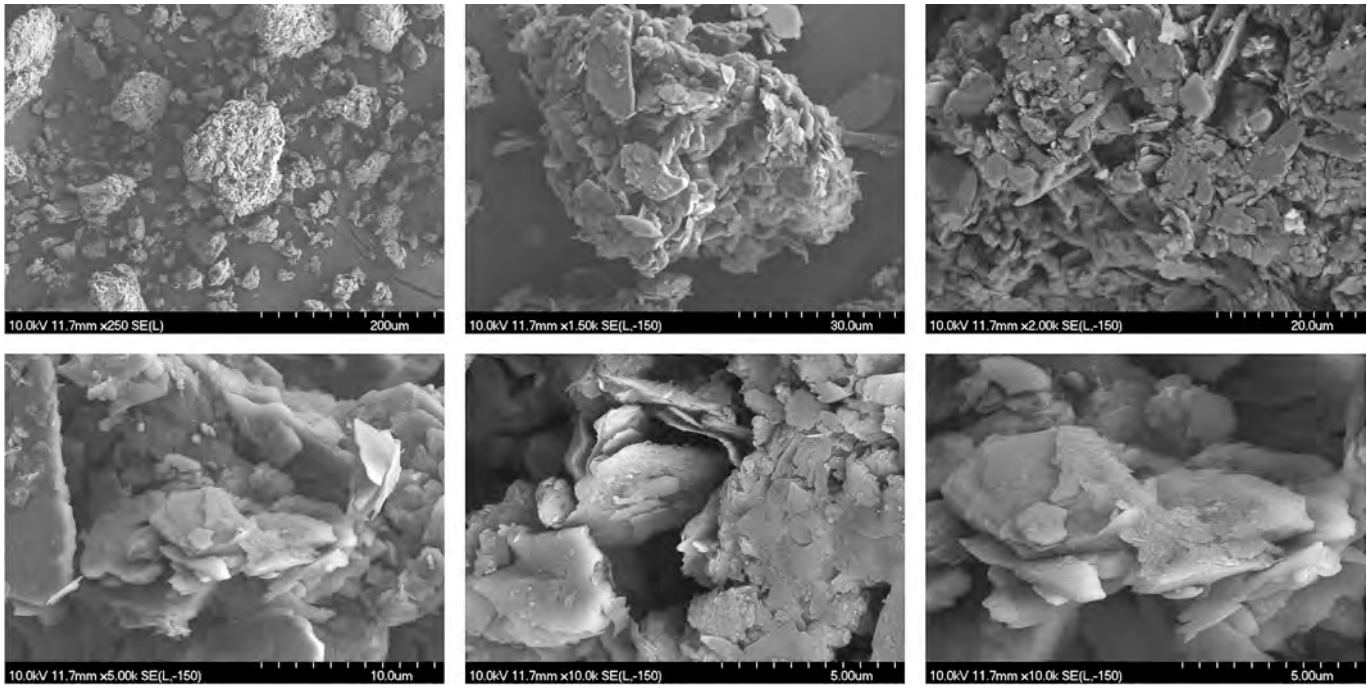

Fig. 9. SEM images at different magnifications showing the morphological characteristics of sample BP-25-2.

material innovation, functional requirements, and regional practices.

Architectural elements—including form, dimensions, materials, and surface treatments—offer critical insights into social behavior, cultural values, and technological knowledge (Winter-Livneh et al., 2013). While many studies emphasize architectural typologies or settlement patterns (Winter-Livneh et al., 2013), fewer focus on the physicochemical and microstructural characterization of building materials, which are essential for understanding the technological capabilities of ancient societies.

This study investigates the construction materials used in the Bocapucheros funerary complex, a Bronze Age monumental site in the Campo de Calatrava region, near the fortified settlement of La Encantada (Granátula de Calatrava, Ciudad Real, Spain, Fig. 1). The use of lime in mortars, plasters, renderings and various structures, such as pavements and walls, has been previously described in La Encantada, although without the presentation of any kind of analysis (Nieto Gallo and Sánchez Meseguer, 1980). The focus of our paper is specifically on the characterization of earthen mortars to evaluate whether lime or other advanced treatments were employed to enhance their performance. Additionally, the properties of the stones used in the masonry are

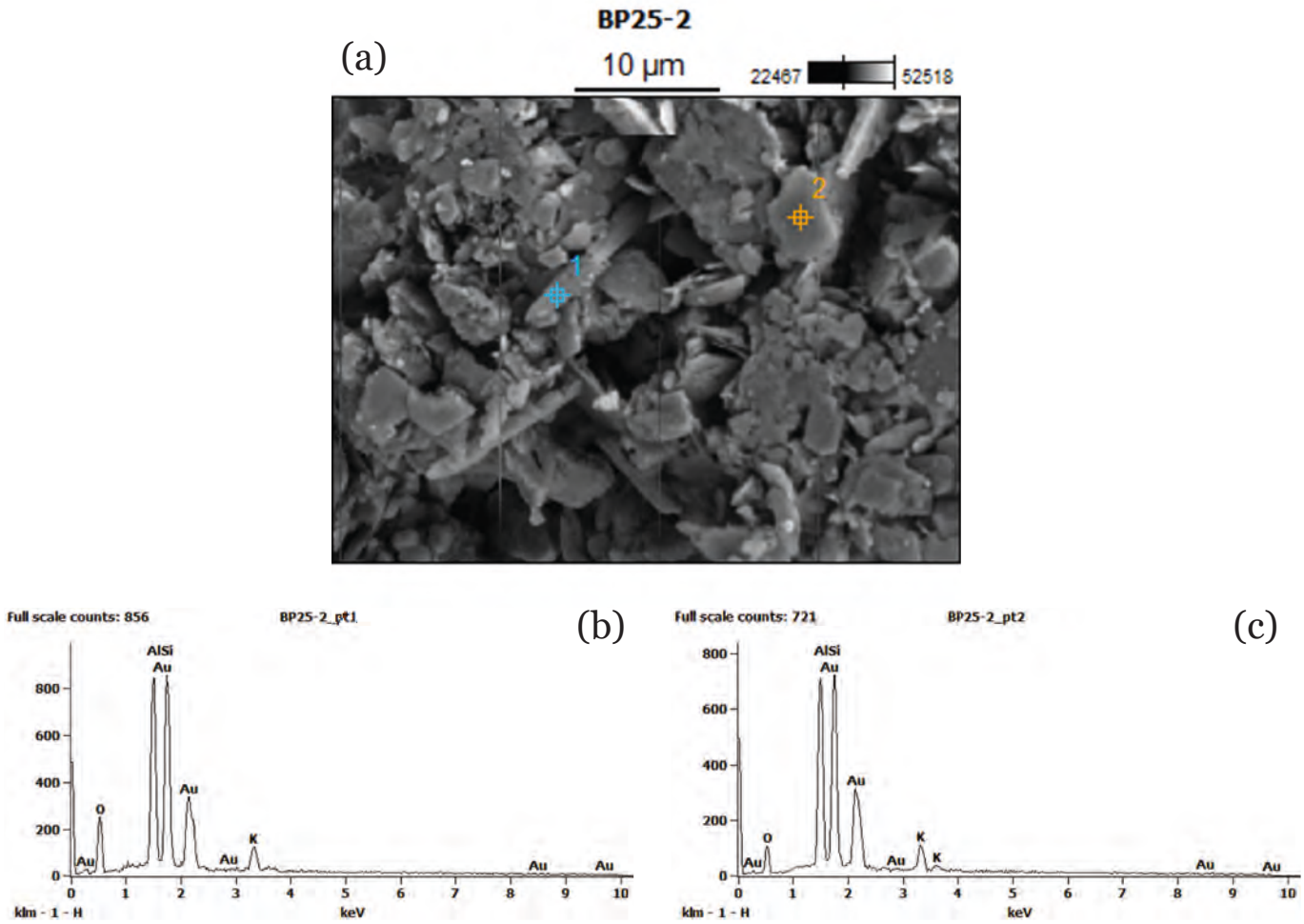

Fig. 10. (a) SEM micrograph of sample BP-25-2; (b) and (c) EDX elemental analyses corresponding to the marked regions.

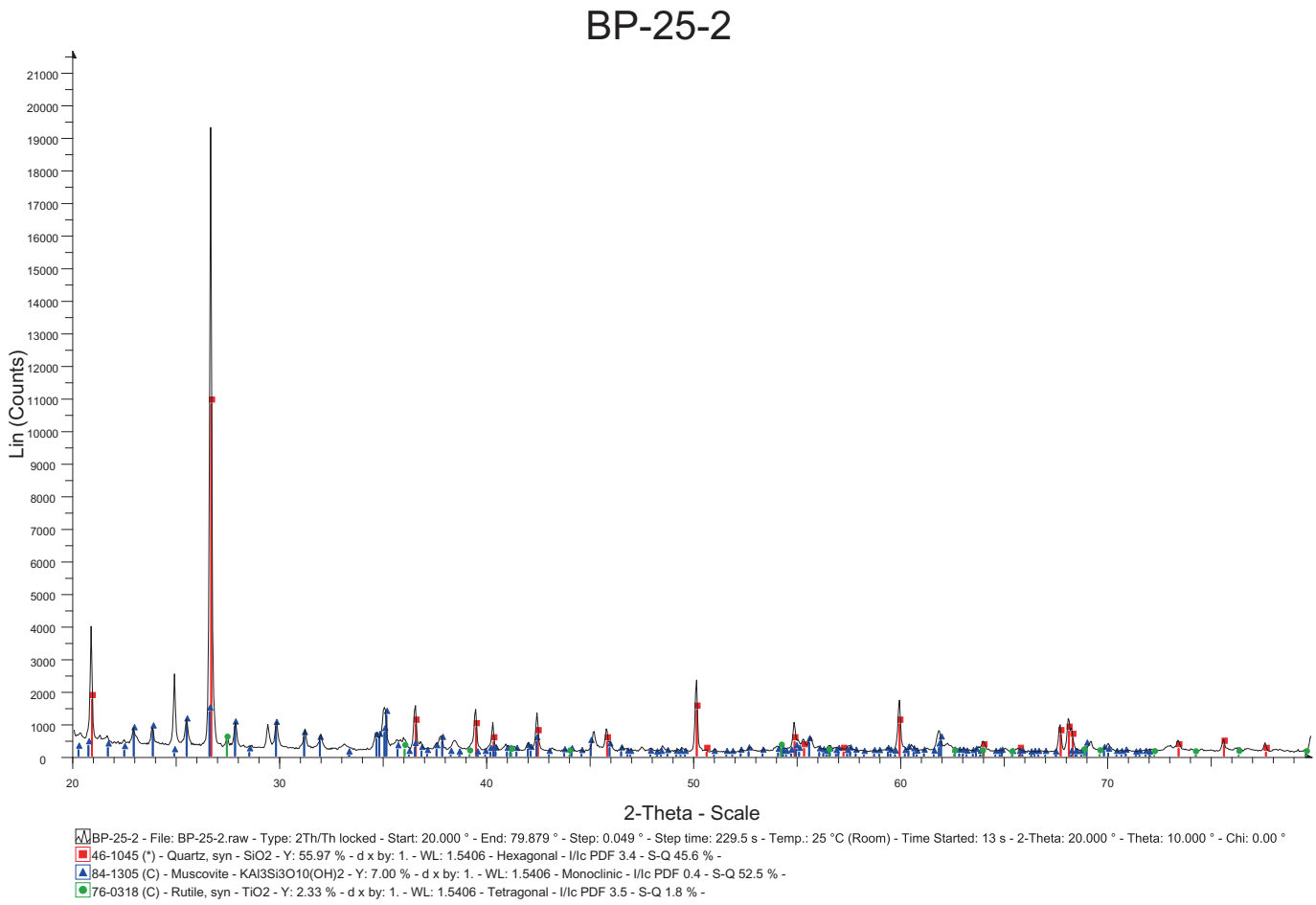

Fig. 11. X-ray diffraction (XRD) analysis of sample BP-25-2.

Table 2
Comparative semi-quantitative XRF analysis of samples BP-25-2, BP-25-3, and BP-25-5, with detection thresholds defined by the significance factor.

Compound	BP-25-2	BP-25-3	BP-25-5	Compound	BP-25-2	BP-25-3	BP-25-5
Na_2O	0.284	0.241	0.330	V_2O_5	0.020	0.022	0.026
MgO	0.735	0.751	0.529	Cr_2O_3	0.020	0.017	0.017
Al_2O_3	23.941	22.691	25.482	MnO	0.028	0.019	0.017
SiO_2	51.764	57.155	55.070	Fe_2O_3	3.534	4.587	4.239
P_2O_5	1.044	0.554	0.474	Co_3O_4	—	0.010	0.010
SO_3	0.230	0.104	0.377	NiO	0.009	0.011	0.011
Cl	0.013	—	0.025	CuO	0.006	0.006	0.005
K_2O	3.943	3.236	4.480	ZnO	0.005	0.004	0.003
CaO	4.444	2.379	0.810	Ga_2O_3	0.004	0.003	0.004
TiO_2	1.270	1.175	1.257	As_2O_3	0.006	0.006	—
Rb_2O	0.014	0.013	0.016	SrO	0.066	0.054	0.060
Y_2O_3	0.004	0.004	0.005	ZrO_2	0.049	0.059	0.053
Nb_2O_5	0.003	0.003	0.003	BaO	0.047	0.036	0.051
CeO_2	0.020	—	—	La_2O_3	—	0.025	—
PbO	0.005	0.003	—	CO_2	8.494	6.832	6.649

examined to contextualize raw material selection and construction techniques. This study presents an integrated methodology that combines geological, physicochemical, and microstructural analyses of construction materials from a prehistoric funerary site. By bridging materials science, Fracture Mechanics, and archaeology, this approach enables a comprehensive interpretation of prehistoric construction techniques and contributes to a deeper understanding of Bronze Age masonry, as well as early earth mortar and concrete technologies.

The originality of this study lies in its multidisciplinary approach, combining materials science and archaeology, to advance the understanding of ancient construction practices. Moreover, studies and analyses of this kind remain relatively uncommon in research on recent prehistoric contexts in Spain (Gómez Morgade et al., 2021) and more broadly in the Iberian Peninsula (Bruno and Faria, 2008; Bruno et al., 2010).

Key contributions include the first-ever characterization of earthen mortars from the Bocapucheros complex to determine the possible use of lime or other additives as binders; the evaluation of raw stone materials and their geological sourcing within the immediate environment; and the assessment of potential binding agents, including lime, using

Table 3
Mineral phases identified by XRD in samples BP-25-2, BP-25-3, and BP-25-5, along with their crystal system and relative abundance (Y).

Sample	Phase	Chemical formula	Crystal system	Percentage (Y)
BP-25-2	Quartz	SiO_2	Hexagonal	55.97%
BP-25-2	Muscovite	$KAl_3Si_3O_{10}(OH)_2$	Monoclinic	7.00%
BP-25-2	Rutile	TiO_2	Tetragonal	2.33%
BP-25-3	Quartz	SiO_2	Hexagonal	81.43%
BP-25-3	Muscovite	$KAl_3Si_3O_{10}(OH)_2$	Monoclinic	10.18%
BP-25-3	Rutile	TiO_2	Tetragonal	1.98%
BP-25-5	Quartz	SiO_2	Hexagonal	50.00%
BP-25-5	Muscovite	$KAl_3Si_3O_{10}(OH)_2$	Monoclinic	6.25%
BP-25-5	Rutile	TiO_2	Tetragonal	2.08%

advanced analytical techniques. These findings aim to provide new evidence on the technological capabilities of Bronze Age communities in the Iberian Peninsula and to refine current interpretations of construction practices in prehistoric monumental architecture.

2. Description of the Bocapucheros archaeological site

The Bocapucheros site, also known as Fuente de los Pucheros (Blanco de la Rubia and Martínez García, 2022), is a monumental Bronze Age funerary complex (19–17 th centuries BC) located in the municipality of Almagro (Ciudad Real, Spain – Fig.2 (a), (b)). It lies in the southern sector of the volcanic Campo de Calatrava region, immediately south of the La Yezosa volcano. Strategically situated on the southern slope of a hillside composed of Ordovician quartzites and pink sandstones—part of the so-called *Purple Series* (Instituto Geológico y Minero de España IGME, 1988)—the site occupies a dominant topographic position, offering extensive visual control over the surrounding landscape (Fig.2 (c), (d)).

This elevated vantage point offers broad visibility toward the south and southwest, across the Jabalón river valley, as well as to the northwest. The visual domain includes lower-altitude areas such as Negrizales Grandes, Haza de Fraguas and Cañada del Gato, extending as far as the Sierra del Moral. The proximity of the Añavate stream, a tributary of the Jabalón, enhances the strategic value of the site, providing both hydrological resources and a strong visual and territorial presence. The site effectively oversees a natural corridor connecting the southern Meseta with Upper Andalusia (Benítez de Lugo Enrich et al., 2021).

The funerary complex was constructed through extensive modification of the original rocky promontory (Benítez de Lugo Enrich et al., 2022). The core area was reshaped to create a levelled platform by

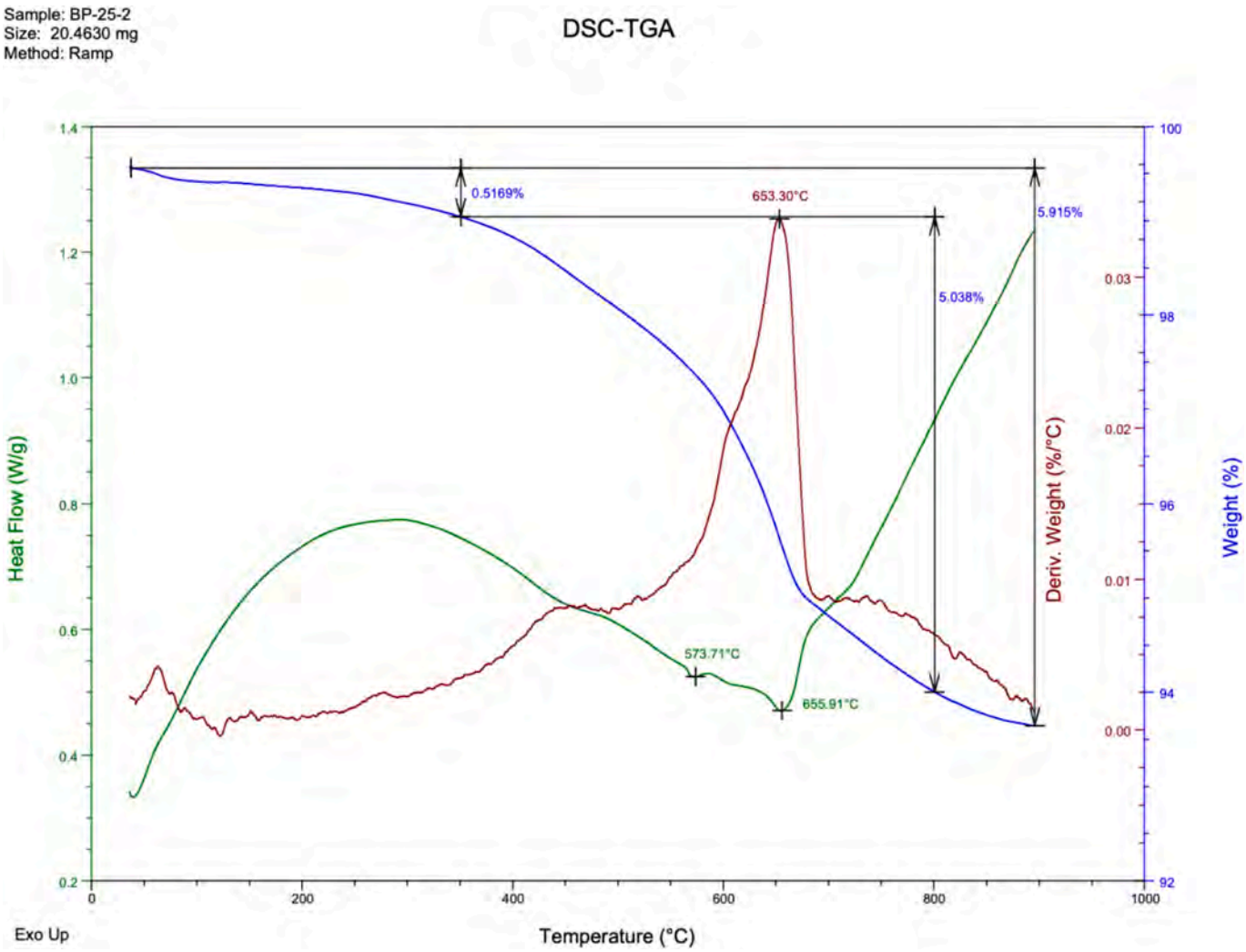

Fig. 12. Thermal analysis of earth-mortar sample BP-25-2.

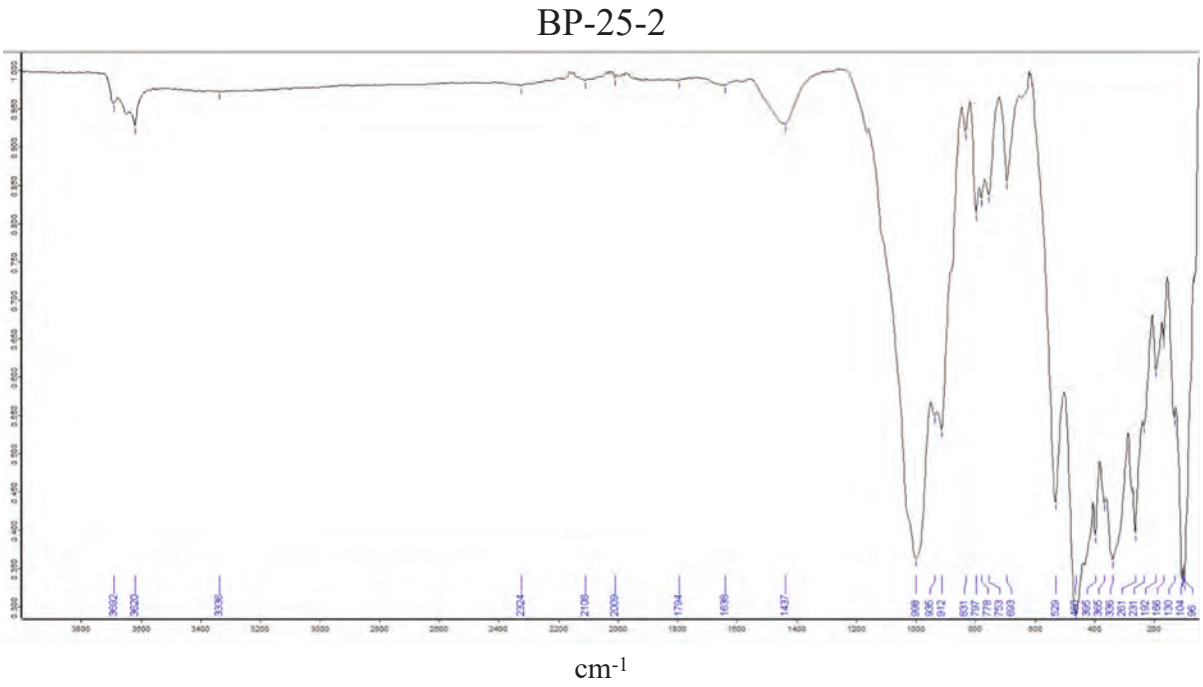

Fig. 13. FTIR spectra of the BP-25-2 sample, highlighting the characteristic vibrational bands used to identify the main mineral phases present in the earth mortars.

systematically carving and terracing the natural quartzite ridge, resulting in an artificial elevation of approximately 10 meters. This intervention provided a stable base for monumental construction while simultaneously enhancing the site's visibility and symbolic prominence.

Various types of masonry structures have been preserved at the site. Architectural features within the complex include a large tumulus (Benítez de Lugo Enrich et al., 2022; Blanco de la Rubia and Martínez García, 2022) with passageways and at least three burial chambers, a central artificial platform, a pentagonal enclosure, a terrace, a cave, two clustered architectural units, and integrated water catchment systems (Benítez de Lugo Enrich et al., 2022). Collectively, these elements reflect a high level of technical sophistication and ritual intentionality, characteristic of Bronze Age funerary landscapes (Benítez de Lugo Enrich et al., 2022). The remains of several individuals have been recovered in and around the burial chambers. Radiocarbon dates have been obtained for two of them (Benítez de Lugo Enrich et al., 2022) (see Table 1). BP-1 was found buried within Chamber 2, whereas BP-2 was discovered out of context—on the surface, rolled and located halfway up the hillside.

The central structure comprises a platform constructed from quartzite blocks of varying dimensions, sourced through the deliberate reduction of the surrounding bedrock. This platform served both structural and symbolic purposes—elevating and stabilizing the terrain to support the superimposed funerary architecture. The tumulus erected atop this foundation features chambers with dry-stone pseudo-vaults and masonry constructed from locally available stone and earthen mortars (Benítez de Lugo Enrich et al., 2022). The construction techniques employed demonstrate advanced knowledge of materials and site planning, revealing the cultural and symbolic complexity of the community responsible for the monument (Benítez de Lugo Enrich and Mejías Moreno, 2017).

3. Materials and methods

3.1. Materials

3.1.1. Stone materials

The monumental complex was built using large stone blocks of variable size extracted and roughly shaped from local bedrock (Fig. 3 (a), (b)). The surrounding geology comprises schists, slates, quartzites, and sandstones of the Purple Series (Lower Ordovician), belonging to the Central Iberian Zone of the Iberian Variscan Massif, together with olivine-bearing basalts associated with the Calatrava Volcanic Field (Villafranchian–Holocene) (Instituto Geológico y Minero de España IGME, 1988). The builders' selection of materials and geometries reflects an empirical optimization of load redistribution and compressive load paths, resulting in structurally robust systems that anticipate fundamental principles of stress management and failure prevention.

3.1.2. Earth mortars

A representative sampling of earth-based mortars was conducted on selected joints of the quartzitic masonry of the monument during the 2024 excavation campaign (Fig. 4). The sampling strategy ensured adequate spatial and stratigraphic coverage to enable analysis of the various construction phases and their microstructural characteristics. Sample BP-25-2 was collected from the lower section of a masonry wall segment located within one of the corridor structures. Sample BP-25-3 was extracted from the base of the masonry wall adjacent to the entrance of one of the funerary chambers. Sample BP-25-5 was obtained from the lower part of the masonry wall inside one of the chambers. It should be clarified at this stage, to avoid confusion, that BP-1 and BP-2 (Table 1) refer to human remains, while BP-25-2, BP-25-3, and BP-25-4 correspond to mortar samples.

3.1.3. Fauna remains consumed

The mortars contain remains of cooked domesticated fauna, identified as ovicaprid fragments and interpreted as food waste discarded by the builders during construction and subsequently incorporated into the mortar matrix. This organic material is archaeologically significant, as it enables radiocarbon dating of the associated inorganic sediment. Isotopic and radiocarbon analyses were conducted on two samples: BP-25-1, an organic carbon stain containing a distal ovicaprid humerus fragment collected from the northern base of the eastern wall of Corridor 1, and BP-25-2, a probable ovicaprid rib fragment recovered from the southern base of the same wall.

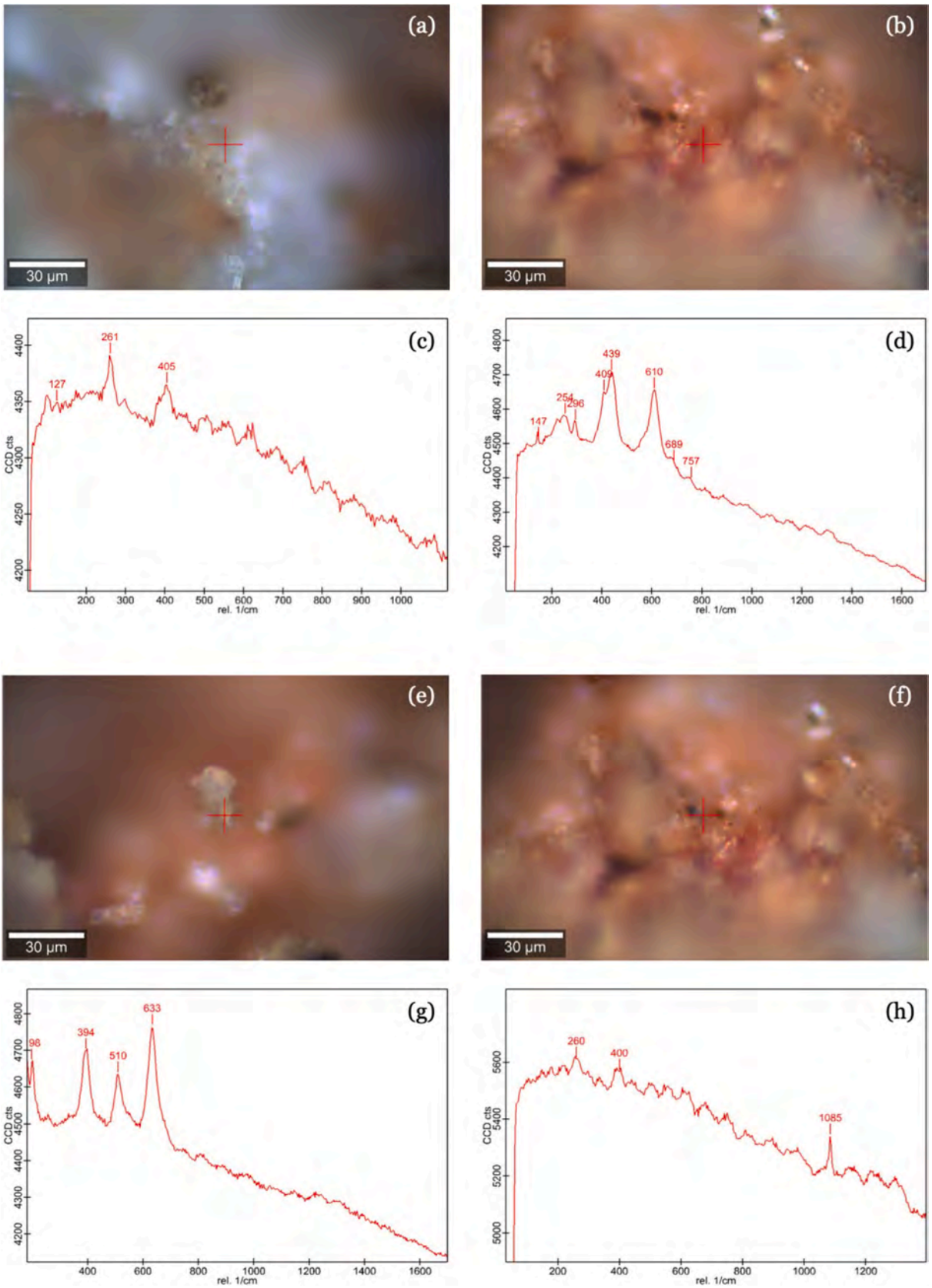

Fig. 14. Raman spectra of sample BP-25-2: (a), (b), (e), and (f) microscope images captured using a reflection microscope; (c), (d), (g), and (h) corresponding Raman spectra.

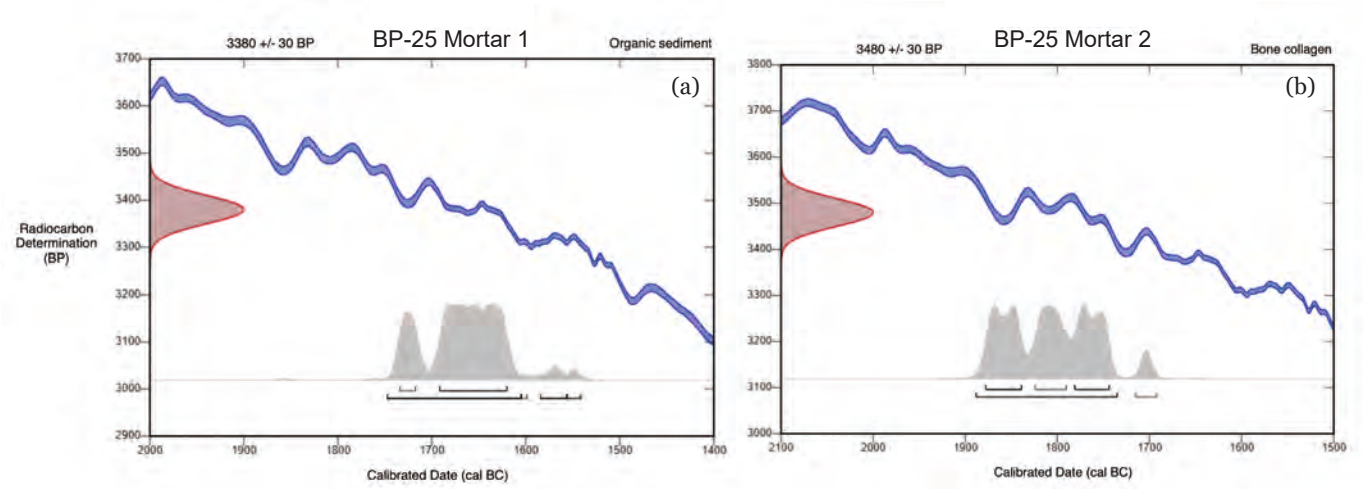

Fig. 15. Calibrated ages of mortars. (a) BP25 Mortar 1 and (b) BP25 Mortar 2, estimated from faunal remains incorporated during the construction of Bocapucheros.

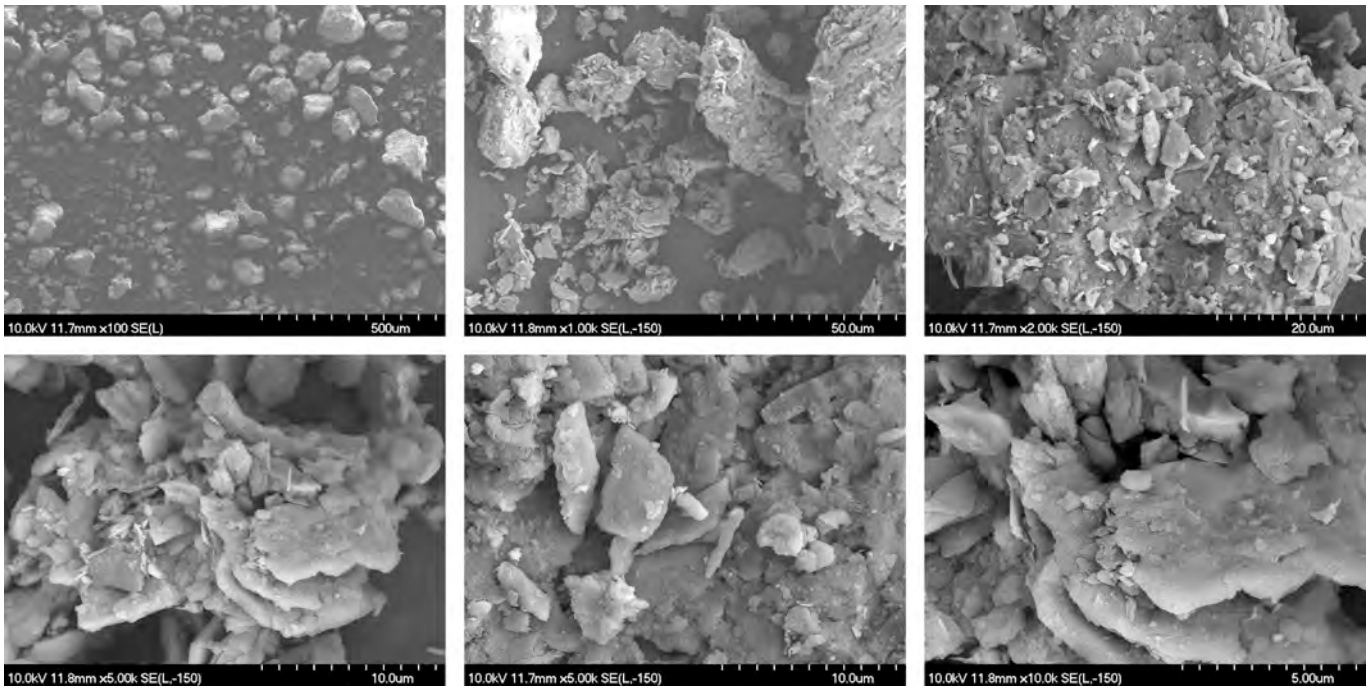

Fig. 16. SEM images at different magnifications showing the morphological characteristics of sample BP-25-3.

3.2. Methods

Masonry stone was assessed through qualitative in situ visual examination, whereas earthen mortars were investigated using combined macroscopic observations and quantitative mineralogical, spectroscopic, thermal, and microstructural analyses. In addition, two previously unpublished radiocarbon dates obtained from cooked ovicaprid remains embedded in the mortars are reported.

3.2.1. Methodologies for the analysis of stone materials used in masonry

Fracture Mechanics provides an effective framework for interpreting quartzite extraction and shaping in Bronze Age megalithic construction, despite the limited number of studies focused specifically on quartzite lintels. Due to pre-existing microcracks and environmental stressors, quartzite is prone to subcritical crack growth and progressive embrittlement under stresses below its fracture toughness, making Fracture Mechanics particularly suitable for assessing the long-term durability and preservation of archaeological stone structures (Chau et al., 2010). Archaeological evidence further indicates that ancient builders empirically exploited fracture principles through controlled crack initiation and propagation using wedges and impact forces (El-Sehily, 2016). At Bocapucheros, natural fracture networks in local quartzite were systematically exploited for block extraction, and typological, use-wear, and diagnostic tool-mark analyses were employed to reconstruct quarrying and stone-working operational sequences and broader construction practices (Boleti, 2018).

3.2.2. Methodologies for the analysis of earth mortars

Earth mortars were characterized using a multidisciplinary analytical approach integrating visual examination, scanning electron microscopy with backscattered electron imaging and energy-dispersive X-ray spectroscopy (SEM–BSE–EDX), X-ray fluorescence (XRF), X-ray diffraction (XRD), thermogravimetric and differential scanning calorimetry analyses (TGA–DSC), Fourier-transform infrared spectroscopy (FTIR),

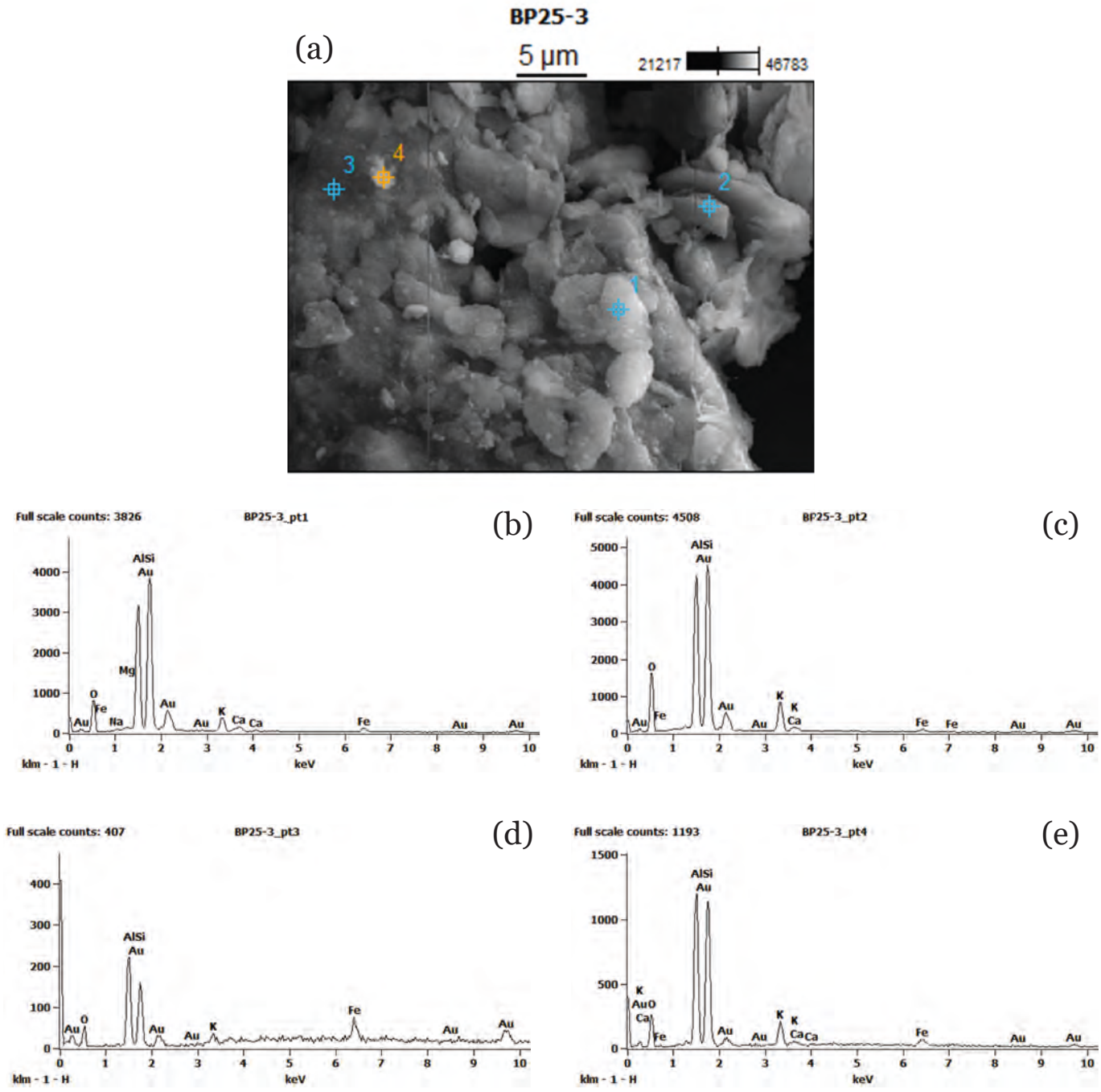

Fig. 17. (a) SEM micrograph of sample BP-25-3; (b)–(e) EDX elemental analyses corresponding to the marked regions.

and Raman spectroscopy. SEM–BSE–EDX analyses were performed using a Zeiss system equipped with an Oxford Instruments detector; bulk chemical composition was assessed by XRF using a Bruker spectrometer; and crystalline phases were identified by XRD using a Bruker D8 Advance diffractometer with CuKα radiation. Thermal behavior was evaluated by TGA–DSC (TA Instruments SDT Q600) under a nitrogen atmosphere, while molecular characterization was conducted by FTIR (Nicolet 6700, KBr pellet method) and Raman spectroscopy (WITec Alpha 300R, 785 nm laser). Radiocarbon and stable isotope (δ^{13} C, δ^{15} N) analyses were carried out at Beta Analytic using NEC accelerator mass spectrometers and Thermo isotope ratio mass spectrometers, following internationally accredited protocols (ISO/IEC 17025:2017).

4. Results and discussion

To enhance clarity and avoid overloading the main text, images from earth mortar samples BP-25-3 and BP-25-5 are presented in the Appendix, whereas those corresponding to BP-25-2 are included in this section.

4.1. Stone materials used in masonry

Fracture Mechanics provides a framework for interpreting quartzite extraction and construction processes at the Bocapucheros monument quarry, where pink quartzite blocks were obtained by exploiting natural fissures in locally available rock formations (Instituto Geológico y Minero de España IGME, 1988). Quarrying likely involved wedges,

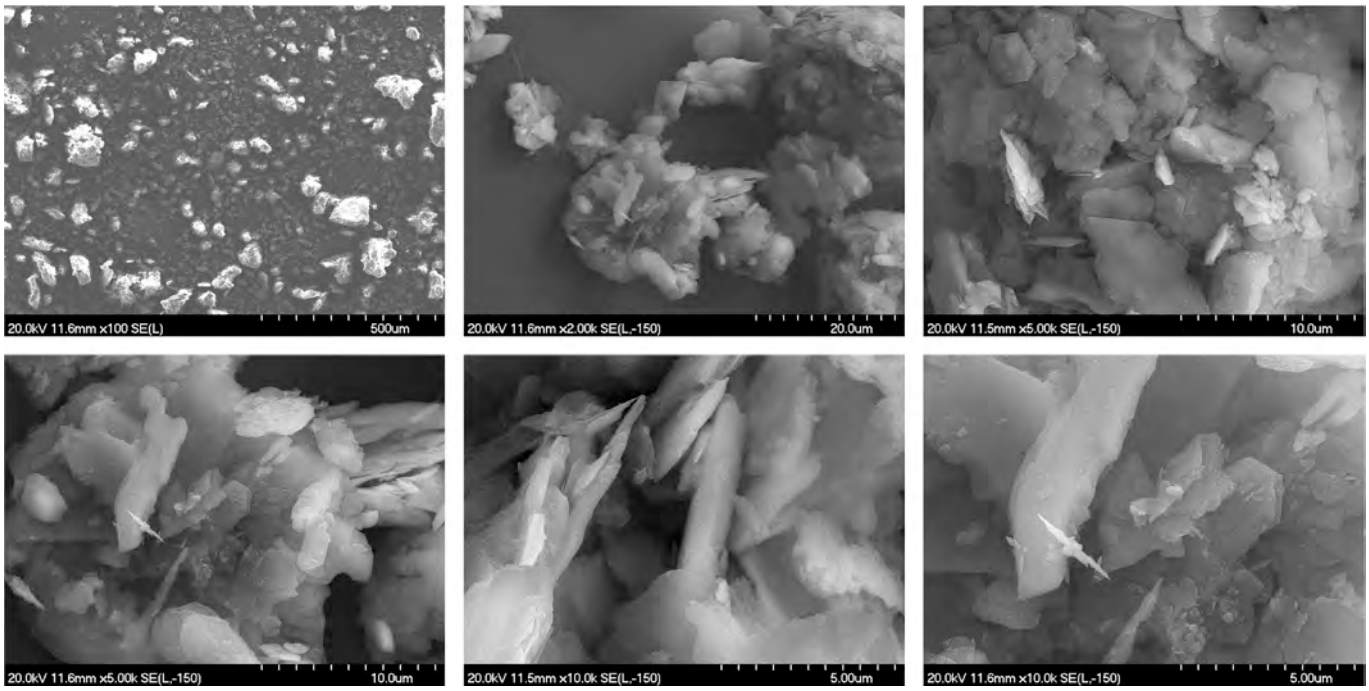

Fig. 18. SEM images at different magnifications showing the morphological characteristics of sample BP-25-5.

chisels, and impact tools, with wooden wedges inducing tensile stresses through swelling to promote controlled crack propagation. Brittle fracture in quartzite is governed by pre-existing microcrack networks that, under wedge-induced tensile stresses, propagate predominantly in mode I, in agreement with Griffith's fracture theory (Griffith, 1920).

The structural system is supported exclusively by load-bearing masonry walls, without internal supports, and incorporates large lintels with oversized cross-sections and redundant bearing elements (Fig. 5 (a), (b)). Fractures are observed in corridor lintels and chamber entrances (Fig. 5), as well as within masonry walls, displaying mode I and mixed-mode (I–II) fracture patterns (Fig. 6 (a)–(c)). These fractures are attributed to time-dependent processes such as differential settlement, partial collapse, or erosion and do not compromise overall structural stability.

The use of irregular polygonal masonry (Figs. 2 and 4) promotes effective load redistribution, reduces stress concentrations, and enhances crack deflection, reflecting an empirical understanding of quartzite fracture behavior comparable to early stoneworking practices documented in other prehistoric contexts (El-Sehily, 2016).

4.1.1. Hypothesized construction sequence and techniques

The hypothesized construction sequence at Bocapucheros, grounded in scientific literature on Bronze Age architectural practices (García Amengual, 2006; Márquez-Romero and Jiménez-Jaimez, 2013; Pastor Quiles, 2021; Sánchez Meseguer et al., 1983) encompasses a multi-phase process reflecting deliberate planning and advanced building methods. The proposed sequence includes:

a) Initial cleaning, clearing, and leveling of the selected site.
b) Preparation of the ground surface to establish a stable foundation.
c) Construction of supporting masonry walls using stone slabs and fragments, arranged to sustain the superstructure.
d) Erection of a low, hemispherical pseudo-dome through concentric corbelling of quartzite slabs bonded with earth mortar.

Archaeological evidence, particularly the collapsed remains of one structure, indicates the use of advanced construction techniques, notably corbelled vaults built without centering through the systematic overlap of beveled stone slabs arranged in radial courses. In some cases, an alternative roofing system consisting of transverse stone slabs sealed with clay or mud layers was employed. The load-bearing system relied exclusively on perimeter masonry walls, without internal supports, reinforcing the monumentality and enclosed character of the funerary spaces (García Amengual, 2006). Earth mortar was selectively used in structurally critical areas such as burial chambers, whereas corridors and lintelled entrances predominantly employed dry interlocking masonry, reflecting a deliberate structural differentiation adapted to functional requirements.

4.1.2. Local stone resources

Understanding the fracture network of a rock mass, including bedding planes, joints, and fissures, is essential for effective quarry planning, as these discontinuities control block size and extraction orientation (Riquelme et al., 2022; Levytskyi et al., 2017). Under these geological conditions, several masonry structures at Bocapucheros were built using locally sourced quartzite, reflecting a strategic use of nearby lithological resources (Fig. 7 (a), (b)). Stone extraction likely involved the insertion of wooden stakes into natural fissures or drilled holes (Fig. 7 (c), (d)), which, upon wetting, generated tensile stresses that facilitated controlled fracturing, followed by block detachment using wedges and levers (García Amengual, 2006). Extracted blocks were transported by human or animal traction or by mechanical means such as rollers and levers, indicating an efficient logistical organization (García Amengual, 2006).

The tumulus was erected on a stepped annular base of dry-stone masonry and earth mortar, and its architectural complexity and construction scale indicate a hierarchically organized society with advanced technical and planning capabilities (Benítez de Lugo Enrich et al., 2022). The monument comprises multiple access corridors and at least three rectangular burial chambers with lintelled entrances, load-bearing masonry walls, and roofing systems capable of sustaining significant superimposed loads. The quartzite lintels function as simply supported beams subjected to bending and tensile stresses; despite visible mode I and mixed-mode cracking, overall structural stability is ensured by compressive loads from the superstructure and lateral confinement by surrounding masonry walls.

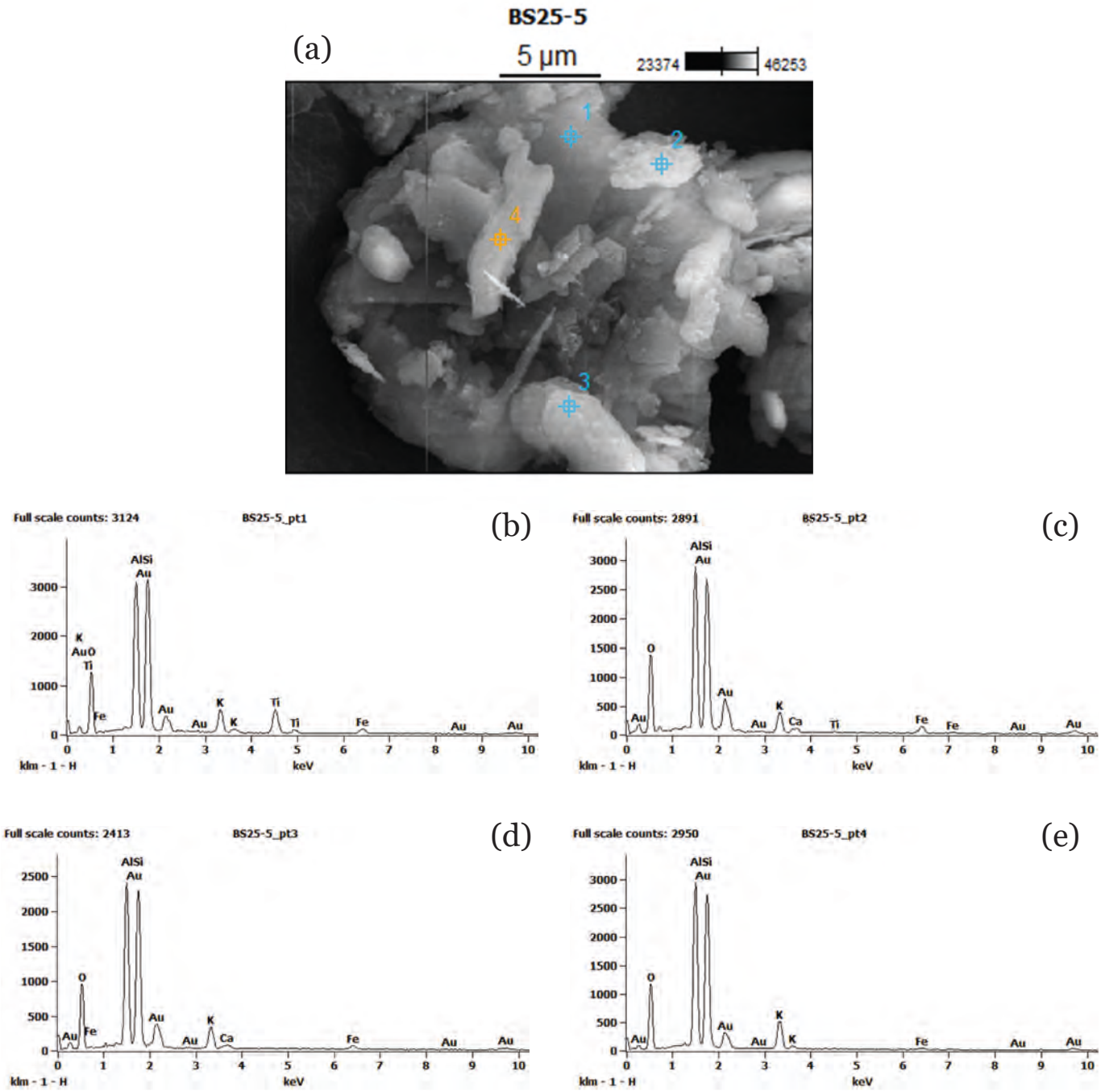

Fig. 19. (a) SEM micrograph of sample BP-25-5; (b)–(e) EDX elemental analyses corresponding to the marked regions.

The structures predominantly employ pink to purplish quartzites from the Purple Series, whose color and fracturability suggest a deliberate balance between aesthetic selection and functional suitability. Evidence of well-developed lichen colonization on quarried and exposed rock surfaces (Fig. 7 (a)–(d)) indicates prolonged surface stability and exposure, consistent with ancient extraction or stone-working activities rather than purely natural processes (Aragón Rubio et al., 2024; Chen et al., 2000). These patterns support the interpretation of anthropogenic modification and long-term weathering of the stone materials. A plausible, though tentative, identification of the observed saxicolous lichen is *Xanthoparmelia pulla*, a widely distributed species in the Iberian Peninsula, noting the high lichen diversity of the Campo de Calatrava region (Calatayud et al., 2011; Becerra-Ramírez et al., 2020; Ancochea and Huertas, 2021).

4.2. Earth mortars

4.2.1. Morphological, grain size, texture, and color analysis

Sample characterization focused on morphology, texture, and color. The overall appearance of samples BP-25-2, BP-25-3, and BP-25-5 is shown in Fig. 8 (a)–(c). The mortars consist of moderately cohesive clay-rich matrices with heterogeneous aggregate grain sizes ranging from millimeter- to centimeter-scale particles, with fine clay fractions promoting aggregate cohesion. Based on granulometric features, some areas, particularly within the tumulus domes, can be classified as earthen concretes rather than simple mortars (Fig. 2).

Sample surfaces are predominantly smooth and rounded, with localized rough and angular textures associated with quartzite aggregates. Minor vacuolar porosity observed in BP-25-3 and BP-25-5 is

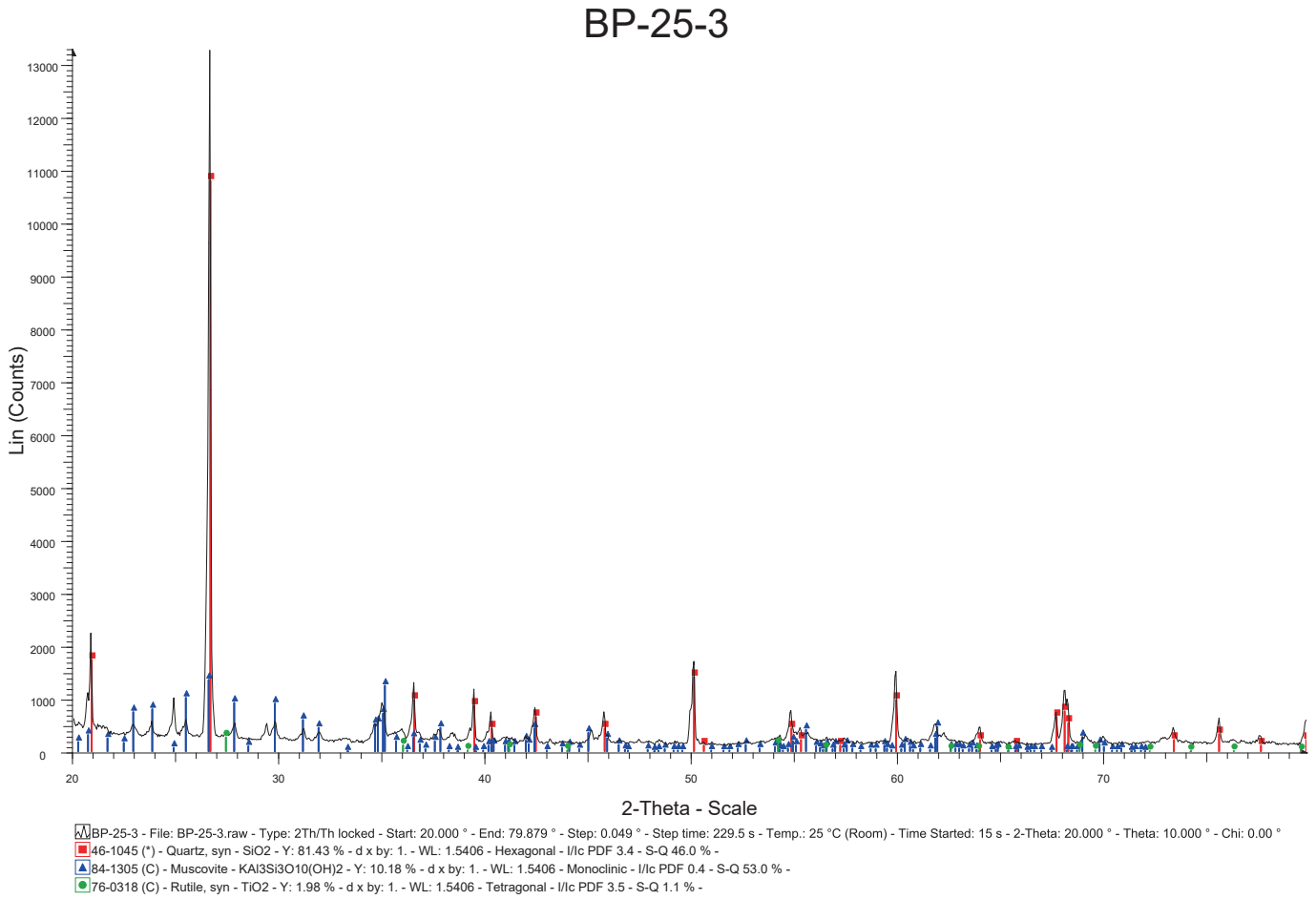

Fig. 20. X-ray diffraction (XRD) analysis of sample BP-25-3.

attributed to drying or shrinkage processes. Chromatically, the mortars exhibit brownish to reddish tones, with occasional lighter particles related to partially altered quartzitic fragments and calcareous crust residues derived from the surrounding soil matrix.

4.2.2. Analysis by scanning electron microscopy (SEM)

Scanning electron microscopy (SEM) was used to examine the microstructure and elemental distribution of samples BP-25-2, BP-25-3, and BP-25-5. SEM–BSE images (Figs. 9, 16, and 18 , the latter two in the Appendix) reveal a heterogeneous elemental distribution and a well-developed lamellar morphology characteristic of clay-based materials, clearly visible from the 30 μm scale and increasingly distinct at 10 and 5 μm.

EDX analyses of BP-25-2 (Fig. 10 (b), (c)) show dominant Al and Si peaks with minor K and O, indicating aluminosilicate-rich clay matrices. Sample BP-25-3 exhibits a broader elemental spectrum, including Mg, Fe, Na, K, and minor Ca in addition to Al and Si (Fig. 17 (b)–(e)), suggesting the incorporation of ferromagnesian phases related to iron-rich clays, with Ca likely derived from carbonation or calcareous soil inclusions. In BP-25-5 (Fig. 19 (b)–(e), Appendix), Al and Si again dominate, with minor Ti, Fe, Na, K, and Ca; Ti is attributed to accessory phases such as anatase, rutile, or ilmenite in volcanic-derived soils.

Overall, SEM–EDX results confirm the predominance of aluminosilicate phases in all samples, with BP-25-3 and BP-25-5 showing greater compositional diversity than BP-25-2, likely reflecting differences in raw material selection, fabrication practices, or post-depositional diagenetic alteration.

4.2.3. X-ray fluorescence (XRF) analysis

Table 2 summarizes the X-ray fluorescence (XRF) results, showing that all samples are dominated by high SiO_2 (51–57%) and Al_2O_3 (22–25%), with notable Fe_2O_3 contents (3.5–4.5%). The relatively elevated iron levels indicate the presence of hematite, confirmed by mineralogical analyses, and possible incorporation into phyllosilicate phases such as muscovite or kaolinite through Al–Fe isomorphic substitution (Álvarez-Rozo et al., 2018). Potassium concentrations correlate with muscovite abundance, whereas Na occurs only in trace amounts, likely related to exchangeable clay cations, minor feldspar inclusions, or the amorphous fraction (Álvarez-Rozo et al., 2018; Bergaya and Lagaly, 2006).

The low CaO contents (0.8–4.4%), together with moderate CO_2 values (6.6–8.5%), indicate that lime was not intentionally added, supporting the interpretation of earth mortars derived from local clay-rich soils, possibly with siliceous sand additions (Álvarez-Rozo et al., 2018). Trace oxides (TiO_2, ZrO_2, V_2O_5) suggest a contribution from weathered volcanic materials consistent with the regional geology, while detectable phosphorus may reflect the incorporation of organic additives of animal origin during mortar preparation.

4.2.4. X-ray diffraction (XRD) analysis

X-ray diffraction (XRD) analysis (Table 3; Figs. 11, 20, and 21, the latter two in the Appendix) confirms muscovite as the dominant phyllosilicate phase in all samples (Álvarez-Rozo et al., 2018; Wilson, 2010). Muscovite, commonly associated with metamorphic and volcanic lithologies, contributes to the plasticity of the mortars (Álvarez-Rozo et al., 2018; González et al., 1983; Lecomte-Nana et al., 2011). Quartz (SiO_2) is also present, derived from both local quartzitic aggregates and

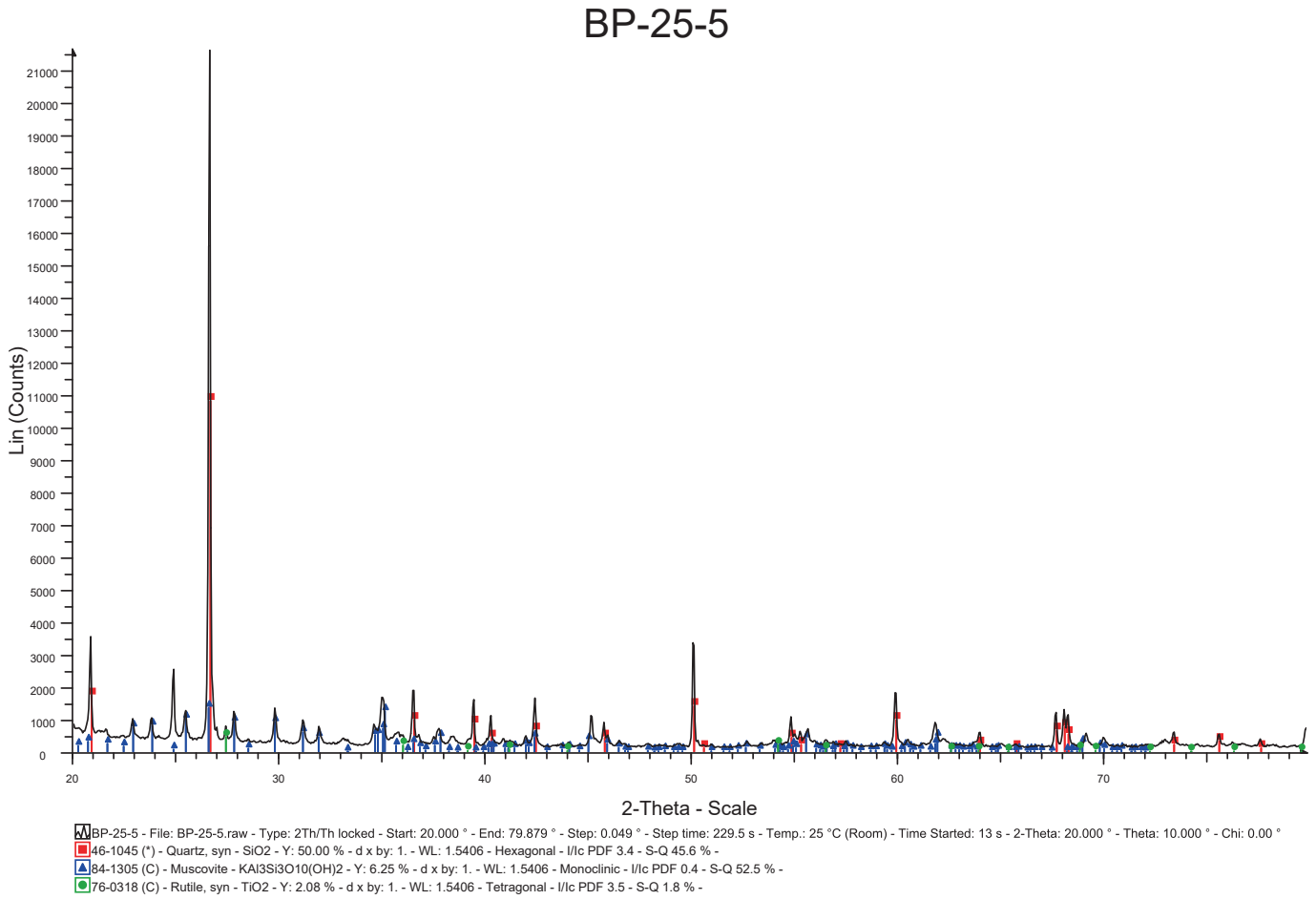

Fig. 21. X-ray diffraction (XRD) analysis of sample BP-25-5.

soil-related components, while rutile (TiO_2) occurs as a minor accessory phase linked to titaniferous minerals or natural pozzolans of volcanic origin. Overall, the mortars are characterized by high phyllosilicate contents, dominated by muscovite, together with substantial quartz proportions, supporting their classification as earth-based mortars.

4.2.4.1. Thermogravimetric analysis and differential scanning calorimetry (TGA–DSC). Figs. 12–23 present the TG–DSC results for samples BP-25-2, BP-25-3, and BP-25-5 (the latter two in the Appendix), while Table 4 summarizes the corresponding mass losses and thermal events. All samples display low total mass losses (≈ 5%), and all thermal events up to 950 °C are endothermic. BP-25-2 shows the highest mass loss (Fig. 12; Table 4), consistent with its higher clay mineral content inferred from XRD data (Table 3) and the hygroscopic behavior of layered phyllosilicates (Álvarez-Rozo et al., 2018; Grim, 1939; Hendricks, 1942).

In BP-25-3, a mass loss near 200 °C (Fig. 22; Table 4) is attributed to dehydration of smectite-group clays, particularly montmorillonite (Álvarez-Rozo et al., 2018; Smykatz-Kloss, 1974; Földvári, 2011). An endothermic peak around 300 °C observed in BP-25-2 and BP-25-5 is associated with hydrated iron phases, such as goethite, rather than organic matter oxidation (Álvarez-Rozo et al., 2018; Smykatz-Kloss, 1974; Földvári, 2011). A further mass loss at 550 °C in BP-25-3 reflects kaolinite dehydroxylation, with possible contributions from muscovite (Álvarez-Rozo et al., 2018; Smykatz-Kloss, 1974; Földvári, 2011). Although muscovite typically dehydroxylates at 820–920 °C, comparable endothermic events were recorded in all samples, consistent with reported reductions in dehydroxylation temperature due to mechanical grinding (Álvarez-Rozo et al., 2018; Rodriguez and Soto, 1991; Mendelovici, 1997; Balek, 2007).

In BP-25-5, a minor mass loss near 700 °C (Fig. 23; Table 4) is attributed to trace calcite. The endothermic peak at 570 °C in all samples corresponds to the α–β quartz transition, while reactions around 650 °C in BP-25-2 and BP-25-3 are linked to the decomposition of minor calcium carbonate (Álvarez-Rozo et al., 2018).

4.2.4.2. Fourier Transform Infrared Spectroscopy (FTIR). Fourier Transform Infrared (FTIR) spectroscopy was used to identify mineral phases in samples BP-25-2, BP-25-3, and BP-25-5 (Figs. 13–25, the latter two in the Appendix). All samples display an absorption band near 455 cm^{-1} attributed to Al–O vibrations in aluminosilicate frameworks, commonly associated with Si–O–Si bending in clay minerals, particularly smectites (Maravelaki et al., 2021; Farmer, 1974). Peaks at 529–530 and 778 cm^{-1} correspond to Si–O bending and stretching modes (García-López et al., 2023; Saikia et al., 2008; Bosch-Reig et al., 2017), while bands near 690 cm^{-1} indicate the presence of anorthite (Maravelaki et al., 2021).

Kaolinite is identified by characteristic bands at 3620, 1000, 790, and 460 cm^{-1} (Maravelaki et al., 2021), and illite is indicated by a distinct absorption at 1638 cm^{-1} in BP-25-2. Diagnostic bands of calcite and aragonite were not detected (Kirboga and Oner, 2013; Maravelaki et al., 2021; Munawaroh et al., 2019; Singh et al., 2016; Toffolo et al., 2019; García-López et al., 2023), indicating the absence of well-crystallized carbonate phases and supporting the interpretation that lime was not intentionally added. Any carbonates observed are therefore attributed to naturally occurring calcium carbonate in the raw materials.

Overall, the FTIR spectra indicate a mineral assemblage dominated by quartz and clay minerals, mainly kaolinite and illite, with only minor poorly crystalline or altered carbonate components.

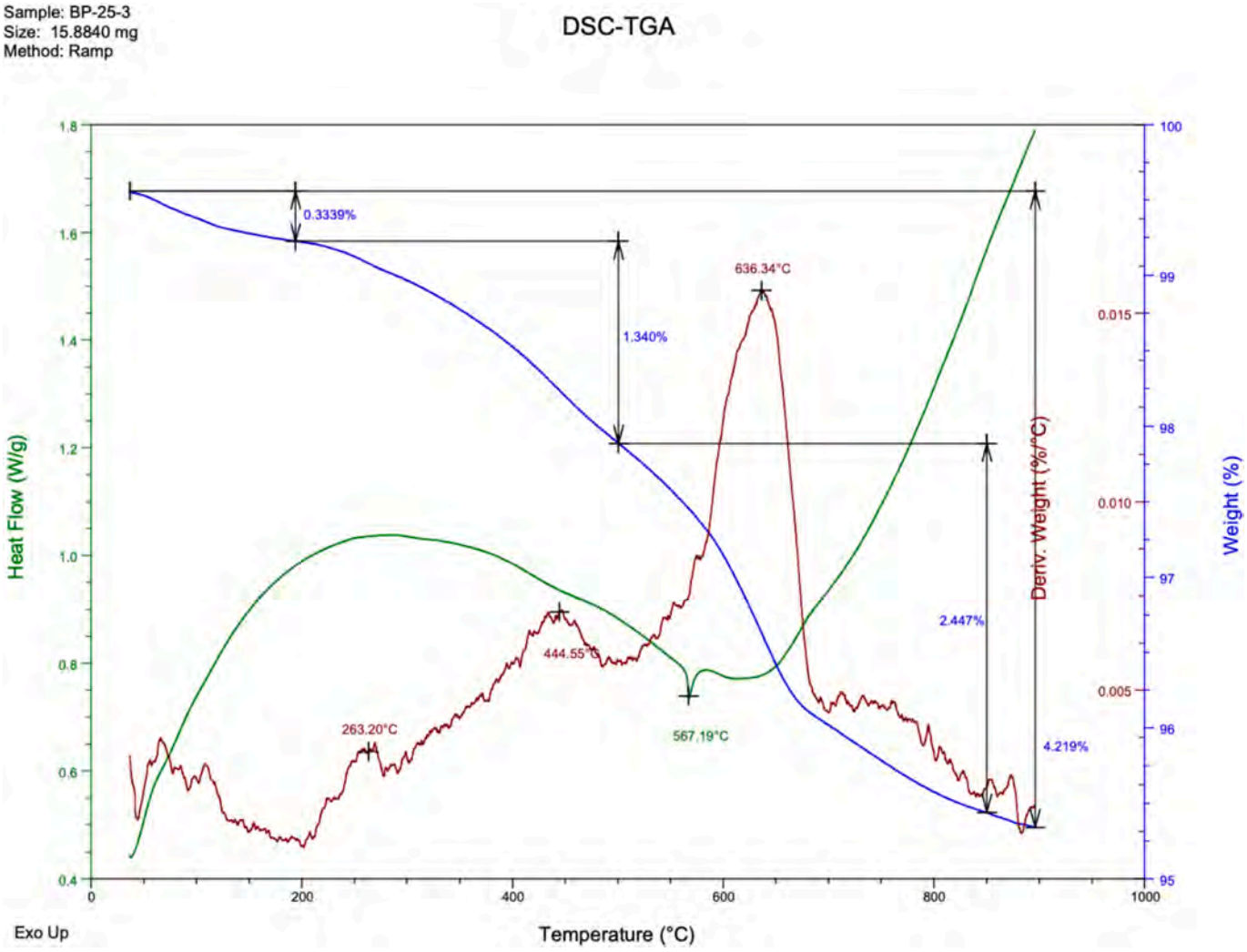

Fig. 22. Thermal analysis of earth-mortar sample BP-25-3.

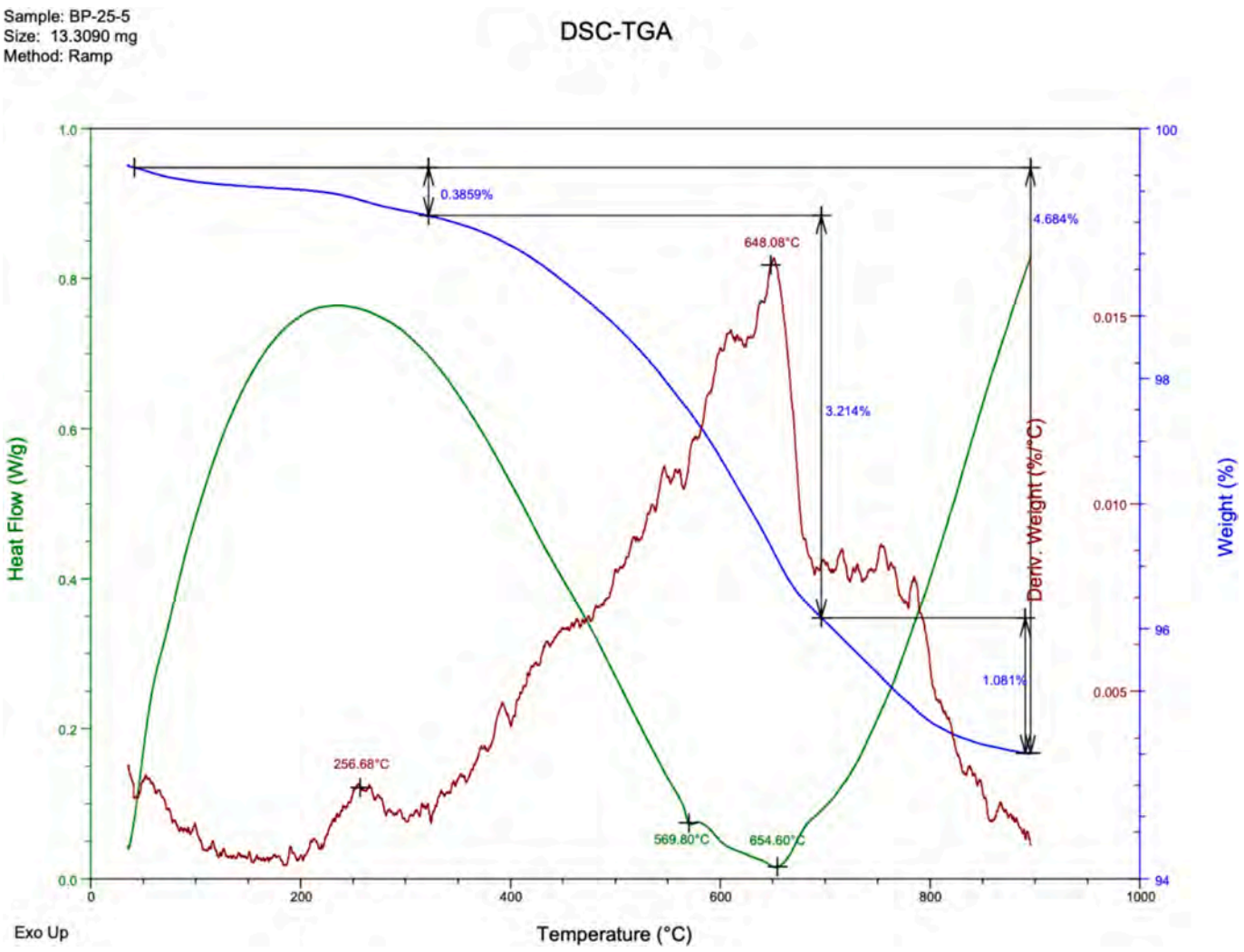

Fig. 23. Thermal analysis of earth-mortar sample BP-25-5.

Table 4
Summary of mass losses from TGA and thermal events observed by DSC in the analyzed samples.

Sample	Temperature range (°C)	Mass loss / Thermal event
BP-25-2	Ambient–400	0.517%
BP-25-2	400–800	5.038%
BP-25-2	800–900	0.360%
BP-25-2	DSC	Endothermic peaks: 573.71 °C, 655.91 °C
BP-25-3	Ambient–200	0.334%
BP-25-3	200–500	1.340%
BP-25-3	500–850	2.447%
BP-25-3	850–900	0.098%
BP-25-3	DSC	Endothermic peak: 567.19 °C
BP-25-5	Ambient–400	0.386%
BP-25-5	400–700	3.214%
BP-25-5	700–900	1.081%
BP-25-5	DSC	Endothermic peaks: 569.80 °C, 654.60 °C

4.2.4.3. Raman Spectroscopy. Raman spectra of samples BP-25-2, BP-25-3, and BP-25-5 are shown in Figs. 14–27 (BP-25-3 and BP-25-5 in the Appendix). All samples display low-frequency bands (<300 cm $^{-1}$) attributed to clay minerals and metal oxides, with additional signals between 400 and 600 cm $^{-1}$ related to silicates, feldspars, and iron-bearing phases. Clay minerals exhibit characteristic Raman-active bands between 170 and 710 cm $^{-1}$, corresponding to internal SiO_4 and Al_2O_3 vibrations, with OH bending modes detected between 840 and 925 cm^{-1} (Tanbakouei and Michalski, 2023).

Kaolinite is identified by diagnostic bands at 141–148, 197–205, 270–277, 394–397, 460–475, 503–515, 633–639, and 745–757 cm^{-1} (Figs. 14–27) (Ikehata et al., 2021), with the prominent 144 cm^{-1} peak attributed to Al_2 OH vibrations (Tanbakouei and Michalski, 2023). Anatase was confirmed by overlapping bands at 141–143, 392–395, 512–514, and 635–636 cm^{-1} (Ikehata et al., 2021). Montmorillonite-related bands occur at 172–176, 199–205, 287–293, 425–441, and 701–710 cm^{-1}, with variations among samples indicating differing smectite contents (Tanbakouei and Michalski, 2023); (Ikehata et al., 2021) . Minor clay phases include palygorskite (180 and 258 cm^{-1}) and hectorite (688 cm^{-1}).

An intense band near 1085 cm^{-1} in BP-25-2 and BP-25-3 is attributed to calcite (Smith et al., 2013). Both anatase and rutile TiO_2 polymorphs are detected through characteristic Ti–O vibrations, while bands at 1309 and 1600 cm^{-1} in BP-25-5 indicate carbonaceous compounds, suggesting the presence of organic carbon-rich material within the mortar matrix (Chen, 2020).

4.2.4.4. Role and application of lime in earthen mortars. Since the Neolithic, earthen mortars have been widely used as binding and protective materials in stone and earthen architecture (Gómez Morgade et al., 2021; Pastor Quiles, 2017; Jover Maestre et al., 2016). A major technological innovation during Late Prehistory was the intentional production and use of lime and gypsum, marking an important step in

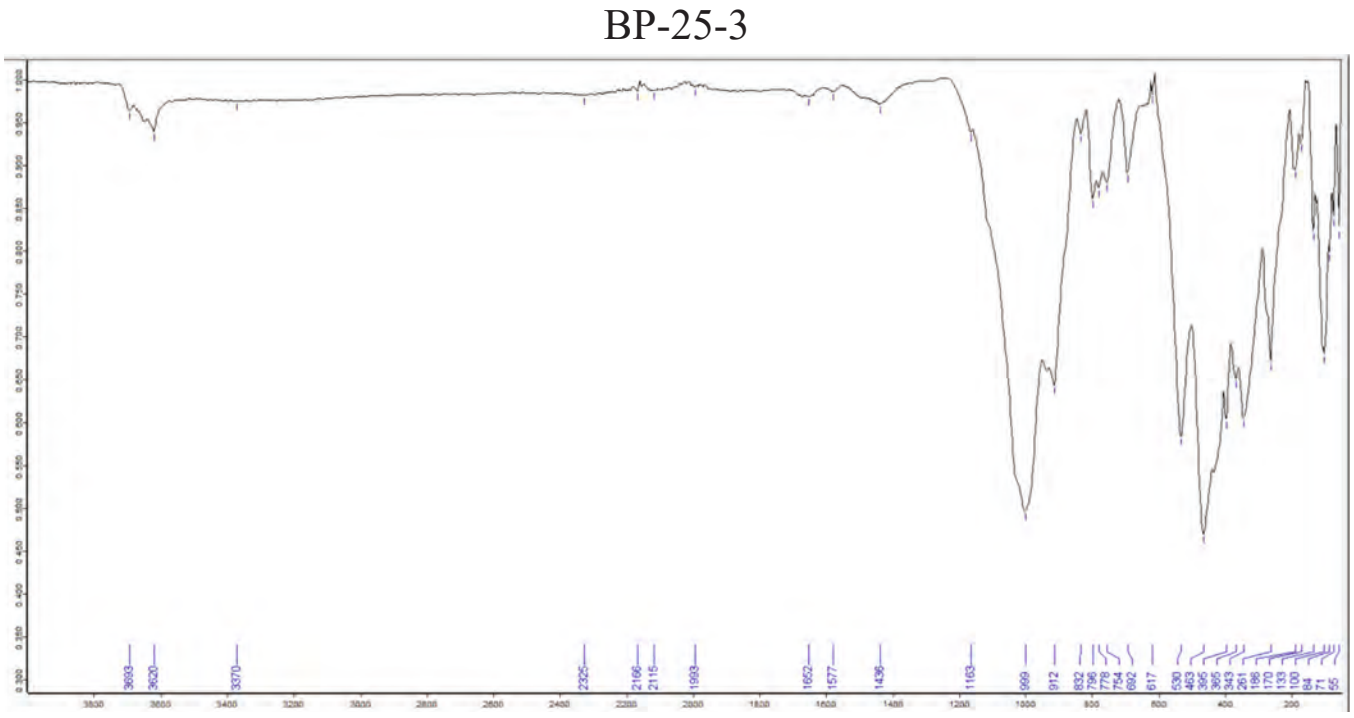

Fig. 24. FTIR spectra of the BP-25-3 mortar sample.

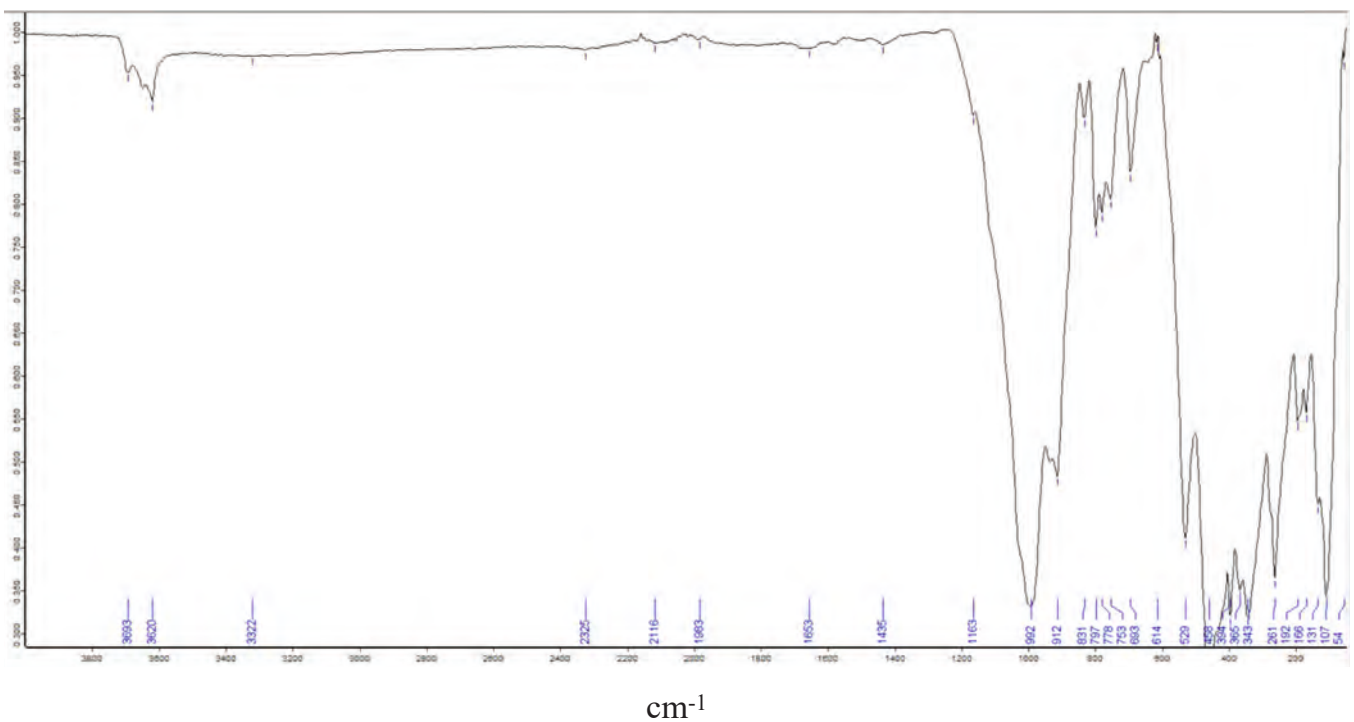

Fig. 25. FTIR spectra of the BP-25-5 mortar sample.

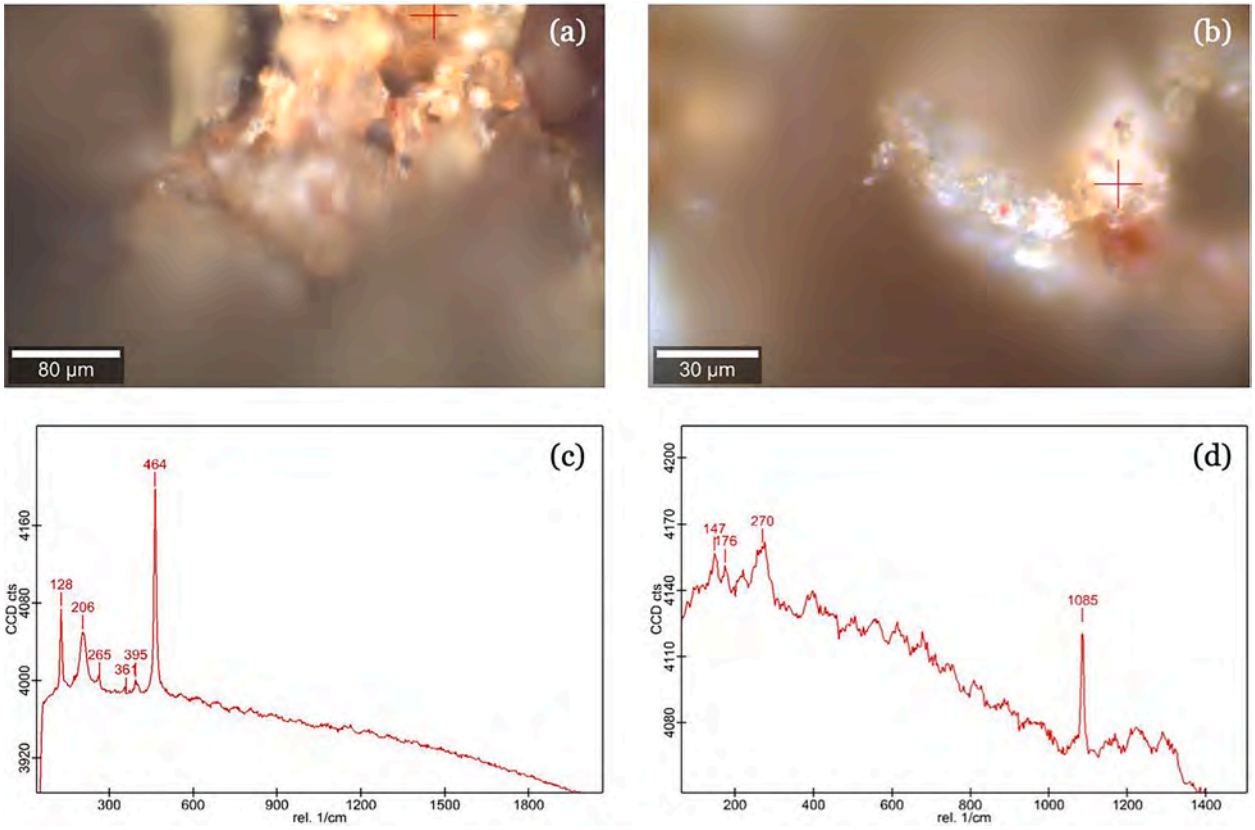

Fig. 26. Raman spectra of sample BP-25-3: (a), (b) microscope images captured using a reflection microscope; (c), (d) corresponding Raman spectra.

material transformation technologies and improving mechanical performance and durability (Brysbaert, 2007; Jover Maestre et al., 2016; Pastor Quiles, 2021; Hobbs and Siddall, 2011). In the Iberian Peninsula, lime use has traditionally been linked to Protohistoric influences from the Eastern Mediterranean (Pastor Quiles, 2021; Díes Cusi et al., 2001), although evidence suggests earlier applications from the late 3rd millennium BCE, with a selective and uneven distribution during the 2nd millennium cal BCE related to functional and social factors (Jover Maestre et al., 2016; Garfinkel, 1987). Notable examples include the clay–lime mortars documented at La Almoloya (Lull et al., 2021), contrasted with sites such as Castro de Santa Trega, where lime is absent and mortars rely exclusively on local raw materials (Gómez Morgade et al., 2021).

Distinguishing intentionally produced lime from naturally occurring carbonates requires a multidisciplinary analytical approach (Jover Maestre et al., 2016). At Bocapucheros, the carbonate phases identified are consistent with raw material sources rather than deliberate lime addition. By contrast, the nearby contemporaneous site of La Encantada shows extensive use of lime plasters in walls, floors, and architectural finishes, including waterproof external coatings and pigmented lime renders (Sánchez Meseguer et al., 2004; Nieto Gallo and Sánchez Meseguer, 1980; Sánchez Meseguer and Galán Saulnier, 2019; Sánchez Meseguer et al., 1983; Sánchez Meseguer and Galán Saulnier, 2001). Although architectural parallels between both sites are plausible, the analytical results indicate that at Bocapucheros lime was not intentionally incorporated into earthen mortars in quantities sufficient to enhance structural performance, suggesting its use—if present—was limited to superficial protective or aesthetic applications.

4.3. Fauna remains integrated in the mortars

Two mortar-associated samples from the funerary tumulus were analyzed: BP-25 Mortar 1 (Beta-755875) and BP-25 Mortar 2 (Beta-755874). The bone from BP-25 Mortar 1, identified as a heat-altered ovicaprid distal humerus, failed to yield a separable collagen fraction due to advanced degradation and could not be dated. Consequently, the surrounding organic sediment was dated following acid pretreatment to remove carbonates. As organic sediments may behave as open systems, the radiocarbon date obtained of BP-24 Mortar 1 sample, 1746 (1685) 1544 BC, reflects the bulk organic carbon matrix rather than a discrete material and should therefore be interpreted with caution. In contrast, the BP-25 Mortar 2 sample, identified as an ovicaprid rib, preserved sufficient collagen for radiocarbon dating. The corresponding radiocarbon and isotopic results are reported in Table 5.

Figure 15 and Table 5 present the calibrated radiocarbon ages obtained from faunal remains incorporated into the mortars. The two new dates are internally consistent and compatible with previously published chronologies. The calibrated ages range between 1887–1695 BC and 1746–1544 BC, and the offset between the two mortar dates suggests that the construction of the funerary tumulus extended over multiple phases. BP-25 Mortar 2 (1887 [1859–1771] 1695 BC) slightly predates the earliest buried individual, BP-1 from Chamber 2 (1884 [1767–1751] 1692 BC), whereas the date of BP-2 (1878 [1741] 1632 BC), recovered out of context, falls between the two mortar dates.

5. Conclusions

This study presents a multidisciplinary investigation and methodology focused on the stone materials and earthen mortars used in the Bronze Age tumular architecture at the Bocapucheros site (Almagro, Ciudad Real, Spain).

The large burial mound of Bocapucheros was built on a natural promontory with excellent visibility to the south and west, particularly the pass connecting the Southern Plateau with Upper Andalusia. Apart from the Bronze Age fortified settlement of Cerro de la Encantada, 6 km away, several motillas (fortified settlements) are located within a day's

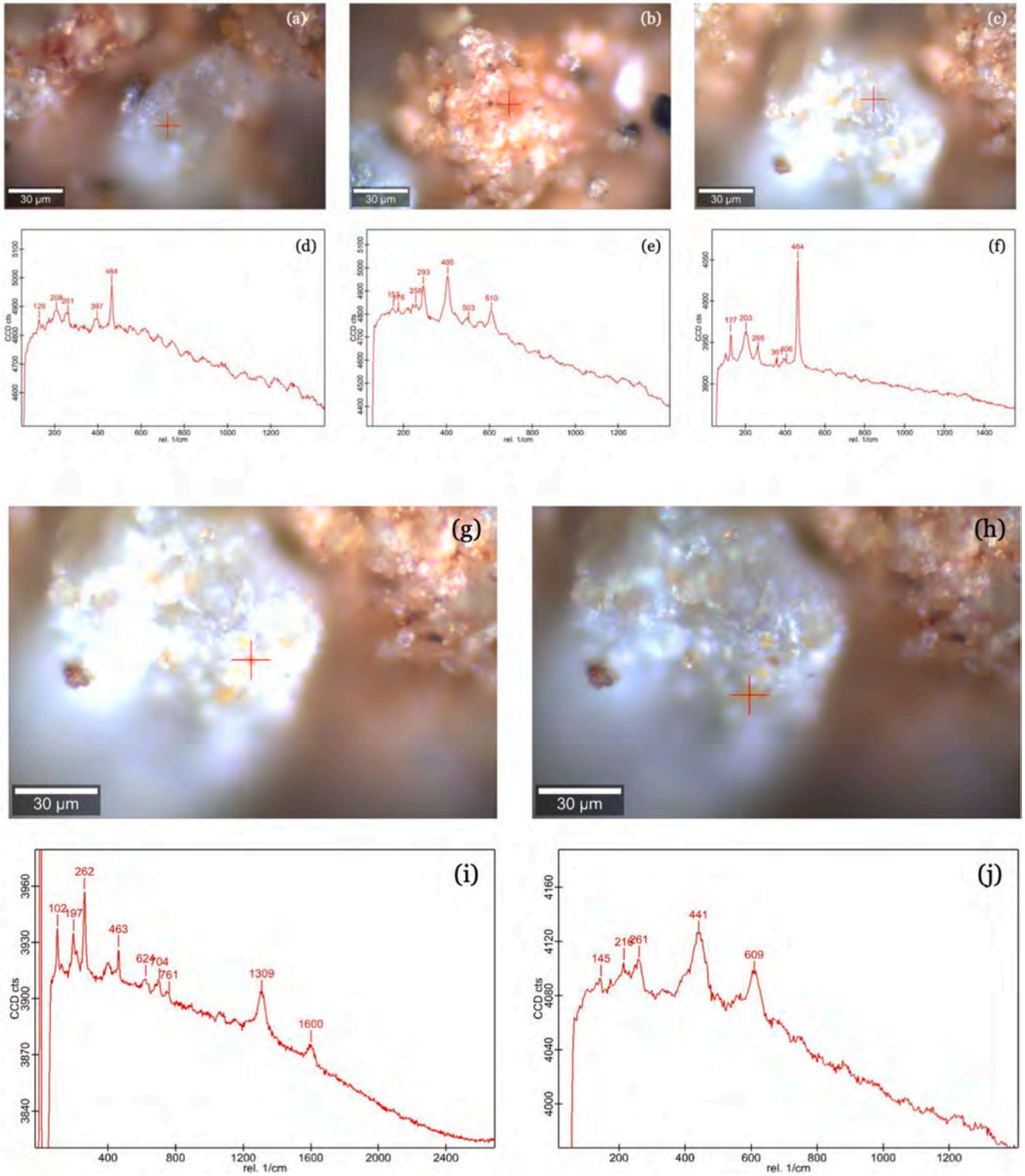

Fig. 27. Raman spectra of sample BP-25-5: (a), (b), (c), (g) and (h) microscope images captured using a reflection microscope; (d), (e), (f), (i) and (j) corresponding Raman spectra.

walk: Los Palacios (Almagro) at 15.4 km, Torralba de Calatrava at 22.9 km, and El Azuer (Daimiel) at 26.7 km. The levelled stone platform on which the mound was built rises 10 m above the natural ridge of roughly hewn quartzite, with a diameter of 30.9 m and an area of 2.344 m^2, occupying the upper and central part of a 3.31-hectare hill. The tumulus features a central corridor 11.8 m long and 1.2 m wide, from which several chambers open, each with an access corridor and lintel entrances. The main chamber is Chamber 2, which was partially looted. It was here that the most superficial individual, BP1, a young adult male, dating to the Bronze Age, 1884-1632 BC. Other chambers include Chamber 3, where in-situ remains of two female burials have been recovered, and Chamber 4, which had also been looted. The

Table 5
Radiocarbon and isotopic results from mortars of the Bocapucheros funerary tumulus (Almagro, Ciudad Real).

Site / context	BP	±	$\delta^{13}C$ / C:N	Max. cal. BC (2σ)	Median	Min. cal. BC (2σ)	Lab. no. & material
North corridor 1, East wall, BP-mortar 2	3480	30	−19.76; 3.3	1887	1859; 1845; 1771	1695	Beta-755874 / Bone (ovicaprid)
North corridor 1, West wall, BP-mortar 1	3380	30	−26.10; —	1746	1685	1544	Beta-755875 / Charcoal–sediments
Chamber 2	3470	30	−18.8; 3.2	1884	1767; 1761; 1751	1692	Beta-574064 / Human bone phalanx (young adult male)
Middle terrace, surface	3440	30	−18.4; 3.3	1878	1741	1632	Beta-604904 / Human bone mandible (mature female)

unexcavated portion of the tumulus suggests the existence of one or two additional burial chambers.

The novelty of this research is highlighted by the integration of archaeological, Fracture Mechanics and Materials Science methodologies, offering valuable insights into ancient building techniques. Moreover, the analysis of earthen mortars and related materials in recent prehistoric contexts of Spain remains a scarcely explored area, underscoring the significance of the findings. The analysis of the masonry stones follows a qualitative approach, based on direct visual inspection conducted in situ. In contrast, the characterization of the earthen mortars combines macroscopic evaluation with a range of quantitative analytical techniques, including mineralogical, spectroscopic, thermal, and microstructural analyses.

The results demonstrate the deliberate selection and processing of local quartzitic blocks, as well as the use of advanced construction techniques, such as corbelled pseudo-domes executed without centering. The identification of tensile and mixed-mode fractures within the stonework provides insight into the long-term mechanical behavior and structural resilience of these load-bearing systems, despite sustained environmental and anthropogenic stresses accumulated over millennia.

The analyzed earthen mortars exhibit a complex aluminosilicate mineralogy, with muscovite as the dominant phase, accompanied by variable amounts of kaolinite, quartz, and calcite. These compositions align with the use of locally sourced clay-rich soils and volcanic additives. Morphological and chemical analyses confirm that the mortars functioned effectively as binding agents, demonstrating tailored formulations adapted to diverse architectural demands. Thermogravimetric and spectroscopic data further corroborate the presence of hydrated minerals and carbonates, both essential for mortar durability and longevity.

Furthermore, the results obtained from the various analytical techniques employed in this study support the conclusion that lime was not intentionally incorporated into the earthen mortars at Bocapucheros. Instead, the detected carbonates—identified through both macroscopic observation and advanced instrumental analyses—are most likely derived from naturally occurring calcium carbonate inherent to the raw materials used in mortar production.

For the first time, prehistoric earth-based mortars have been directly dated using radiocarbon methods, providing a robust chronological framework. The dated mortar construction phase, 1887–1695 BC (median probability 1859–1771 BC), is likely earlier than the dated individual buried in the main chamber (Chamber 2), 1884–1692 BC (median probability 1767–1751 BC).

Finally, this study demonstrates how combining Fracture Mechanics and Materials Science with archaeological toolmark analysis can provide a precise understanding of prehistoric buildings' materials and construction processes. This interdisciplinary approach not only enables the reconstruction of ancient building techniques in the absence of textual or iconographic evidence but also underscores the continuing relevance of mechanical and materials science for the study and conservation of ancient architecture.

Declaration of generative AI and AI-assisted technologies in the writing process

The authors acknowledge utilizing ChatGPT-4, an AI-driven language assistant, to enhance the clarity and linguistic quality of this manuscript. The entire content was carefully reviewed and modified by the authors, who retain full accountability for the final submitted version.

CRediT authorship contribution statement

Ángel De La Rosa Velasco: Conceptualization, Data curation, Formal analysis, Funding acquisition, Investigation, Methodology, Resources, Software, Supervision, Validation, Visualization, Writing – original draft, Writing – review & editing. **Luis Benítez de Lugo Enrich:** Conceptualization, Data curation, Formal analysis, Funding acquisition, Investigation, Methodology, Project administration, Resources, Software, Supervision, Validation, Visualization, Writing – original draft, Writing – review & editing. **Alfredo Mederos Martín:** Conceptualization, Data curation, Formal analysis, Funding acquisition, Investigation, Methodology, Project administration, Resources, Software, Supervision, Validation, Visualization, Writing – original draft, Writing – review & editing. **Jesús Rodríguez Pérez:** Data curation, Formal analysis, Investigation, Methodology, Resources, Writing – review & editing. **Gonzalo Ruiz:** Data curation, Formal analysis, Investigation, Resources, Writing – review & editing. **Rodrigo Moreno:** Data curation, Formal analysis, Investigation, Methodology, Resources, Writing – review & editing.

Declaration of competing interest

The authors state that they have no financial conflicts of interest or personal connections that might have influenced the results presented in this study.

Acknowledgements

Archaeological research at Bocapucheros is funded by the Regional Government of Castilla-La Mancha, the E2IN2 company and the City Council of Almagro. Dr. Nuria García García, biologist, paleontologist, and professor at the Complutense University of Madrid, carried out the taxonomic identification of the analyzed faunal remains. The authors would like to express their sincere gratitude to Dámaso Gómez Camacho, owner of Bocapucheros, and his family for their invaluable collaboration and authorization to carry out this research.

Appendix

The present Appendix contains images obtained from different analyses conducted on samples BP-25-3 and BP-25-5.

Analysis by Scanning Electron Microscopy (SEM)

X-ray diffraction (XRD) analysis

Thermogravimetric analysis and differential scanning calorimetry (TGA–DSC)

Fourier Transform Infrared Spectroscopy (FTIR)

Raman Spectroscopy

Appendix A. Supplementary data

Supplementary data to this article can be found online at https://doi.org/10.1016/j.jasrep.2026.105608.

Data availability

Data will be made available on request.

References

Álvarez-Rozo, D.C., Sánchez-Molina, J., Corpas-Iglesias, F.A., Gelves, F., 2018. Características de las materias primas usadas por las empresas del sector cerámico del área metropolitana de cúcuta (colombia). Boletín de la Sociedad Española de Cerámica y Vidrio 57 (6), 247–256. https://doi.org/10.1016/j.bsecv.2018.04.002.

Ancochea, E., Huertas, M.J., 2021. Radiometric ages and time–space distribution of volcanism in the Campo de Calatrava Volcanic Field (Iberian Peninsula). Journal of Iberian Geology 47, 209–223. https://doi.org/10.1007/s41513-021-00167-y.

Aragón Rubio, G., Giménez, G.F., Negrón, V., Vicente, M., Rincón, M., 2024. La conquista silenciosa de los líquenes en los volcanes del Campo de Calatrava. Revista Medio Ambiente Castilla-La Mancha 38.

Balek, V., et al., 2007. Effect of grinding on thermal reactivity of ceramic clay minerals. Journal of Thermal Analysis and Calorimetry 88 (1), 87–91.

Becerra-Ramírez, R., Gosálvez, R.U., Escobar, E., González, E., Serrano-Patón, M., Guevara, D., 2020. Characterization and Geotourist Resources of the Campo de Calatrava Volcanic Region (Ciudad Real, Castilla-La Mancha, Spain) to Develop a UNESCO Global Geopark Project. Geosciences 10 (11), 441. https://doi.org/10.3390/geosciences10110441.

Benítez de Lugo Enrich, L., Mejías Moreno, M., 2017. The hydrogeological and paleoclimatic factors in bronze age motillas culture of la mancha: The first hydraulic culture in europe. Hydrogeology Journal 25 (7), 1931–1950. https://doi.org/10.1007/s10040-017-1607-z.

Benítez de Lugo Enrich, L., Mederos Martín, A., Esteban, C., Fuentes, C., Galindo, M.A., Menchén, G., Moraleda, J., 2022. Bocapucheros (Almagro, Ciudad Real): Nuevo tipo de enterramiento tumular en la Cultura de las Motillas. Spal 31 (2), 31–74. https://doi.org/10.12795/spal.2022.i31.19.

Bergaya, F., Lagaly, G., 2006. Handbook of clay science. In: Developments in clay science, vol. 1. Elsevier Ltd, Amsterdam, Netherlands, pp. 1–18.

Blanco de la Rubia, I., Martínez García, J., 2022. La Edad del Bronce en la cuenca baja del río Jabalón: Estructuras tumulares y fortificaciones en altura, una complejidad manifiesta. Cuadernos de Prehistoria y Arqueología de la Universidad de Granada 32, 299–339. https://doi.org/10.30827/cpag.v32i0.26713.

Boleti, A., 2018. Stone Tools related to Stone Masonry Techniques in the Eastern Mediterranean Bronze Age: An overview. In: ASHLAR. Exploring the materiality of cut-stone masonry in the eastern mediterranean bronze age. Louvain-la-Neuve, Belgium, pp. 241–264.

Bosch-Reig, F., Gimeno-Adelantado, J.V., Bosch-Mossi, F., Doménech-Carbó, A., 2017. Quantification of minerals from ATR-FTIR spectra with spectral interferences using the MRC method. Spectrochimica Acta Part A: Molecular and Biomolecular Spectroscopy 181, 7–12. https://doi.org/10.1016/j.saa.2017.02.012.

Bruno, P., Faria, P., 2008. Earth mortars use on neolithic domestic structures: Some case studies in alentejo, portugal / argamassas de terra em estruturas domésticas do neolítico: Alguns casos de estudo no alentejo, portugal. Conservar Património 8, 5–12.

Bruno, P., Faria, P., Candeias, A., Mirão, J., 2010. Earth mortars use on pre-historic habitat structures in south portugal: Case studies. Journal of Iberian Archaeology 13, 51–67.

Brysbaert, A., 2007. Murex uses in plaster features in the Aegean and Eastern Mediterranean Bronze Age. Mediterranean Archaeology and Archaeometry 7 (2), 29–51.

Calatayud, V., Corrales, J.M., Hernández, S., 2011. Guía de los líquenes del Parque Nacional de Monfragüe. Universidad de Extremadura, Servicio de Publicaciones, Cáceres.

Chau, K.T., Wong, R.H.C., Wong, T.F., 2010. Subcritical cracking: A cause of rock panel failure in buildings. In: Kourkoulis, S.K. (Ed.), Fracture and failure of natural building stones: Applications in the restoration of ancient monuments. Springer, Dordrecht, The Netherlands, pp. 5–18. Available: https://www.springer.com/gp/book/9781402050763.

Chen, N., et al., 2020. Porous carbon nanowire array for surface-enhanced raman spectroscopy. Nature Communications 11, 4772. https://doi.org/10.1038/s41467-020-18561-3.

Chen, J., Blume, H.P., Beyer, L., 2000. Weathering of rocks induced by lichen colonization — a review. Catena 39 (2), 121–146. https://doi.org/10.1016/S0341-8162(99)00085-5.

De la Peña, A., 1992. Castro de torroso (mos, pontevedra). Síntesis de las memorias de las campañas de excavaciones 1984-1990. In: Arqueoloxía/memorias, vol. 11. Xunta de Galicia, Consellería de Cultura e Xuventude, Dirección Xeral do Patrimonio Histórico e Documental.

Díaz del Río Español, P., 2004. Faccionalismo y trabajo colectivo durante la Edad del Cobre peninsular. Trabajos de Prehistoria 61 (2), 85–98.

Díes Cusi, E., 2001. La influencia de la arquitectura fenicia en las arquitecturas indígenas de la Península Ibérica (s. VIII-VII). In: Arquitectura oriental y orientalizante en la Península. Centro de Estudios del Próximo Oriente-CSIC, Madrid, pp. 69–122.

El-Sehily, B.M., 2016. Fracture Mechanics in Ancient Egypt. Procedia Structural Integrity 2, 2921–2928. https://doi.org/10.1016/j.prostr.2016.06.365.

Estudio Arqueología, 2025. Estudio arqueología - arqueología, patrimonio y restauración. Available: https://www.estudio-arqueologia.es/.

Farmer, V.C., 1974. Infrared spectra of minerals. Mineralogical Society, London.

Földvári, M., 2011. Handbook of the thermogravimetric system of minerals and its use in geological practice. In: Occasional papers of the geological institute of hungary, no. 213, p. 180.

García Amengual, E., 2006. El proceso constructivo de un edificio de la Edad del Bronce en Menorca, 31. El caso de Son Marcer de Baix (Ferreries, Menorca), Mayurqa, pp. 113–136.

García-López, A., Dorado Alejos, A., Moratalla Jávega, J., 2023. Explotación de la Piedra en la Protohistoria Ibérica: Análisis FTIR en la Sierra de Alcaraz (Albacete, España) / Stone Exploitation in Iberian Protohistory: FTIR Analysis from the Sierra de Alcaraz, Albacete, Spain. Arqueología Iberoamericana 51, 119–125.

Garfinkel, Y., 1987. Burnt Lime Products and Social Implications in the Pre-Pottery Neolithic B Villages of the Near East. Paléorient 13 (1), 69–76.

Gómez Morgade, T., Rivas Brea, T., Carrera-Ramírez, F., Barbi Alonso, V., 2021. Earth mortars in the 'Castro de Santa Trega' (A Guarda, Pontevedra, Spain). Journal of Archaeological Science: Reports 37, 102931. https://doi.org/10.1016/j.jasrep.2021.102931.

González, J.L., García, F.H., Martínez, J.C., 1983. La arcilla como material cerámico. Características y comportamiento. Cuadernos de Prehistoria y Arqueología de la Universidad de Granada 8, 479–490.

Griffith, A.A., 1920. The phenomena of rupture and flow in solids. Transactions of the Royal Society of London, Series A, Containing Papers of a Mathematical or Physical Character 221, 163–198.

Grim, R.E., 1939. Relation of the composition to the properties of clays. Journal of the American Ceramic Society 22 (1–12), 141–151.

Hendricks, S.B., 1942. Lattice structure of clay minerals and some properties of clays. Journal of Geology 50 (3), 276–290.

Hobbs, L.W., Siddall, R., 2011. Cementitious materials of the ancient world. In: Ringbom, Å., Hohlfelder, R.L. (Eds.), Building Roma aeterna: current research on Roman mortar and concrete. The finnish society of sciences and letters, vol. 128. Helsinki, pp. 35–60.

Ikehata, K., Arakawa, Y., Ishibashi, J., 2021. Raman microspectroscopic study of reference clay minerals and alteration minerals in volcanic ejecta from the 7 March 2012 phreatic eruption on ioto island (iwo-jima), izu-bonin arc, japan. Vibrational Spectroscopy 114, 103247. https://doi.org/10.1016/j.vibspec.2021.103247.

Instituto Geológico y Minero de España (IGME), 1988. Mapa geológico de España: Hoja Almagro. Centro de Publicaciones, Ministerio de Industria y Energía, Madrid.

Jover Maestre, F.J., Pastor Quiles, M., Martínez Mira, I., Vilaplana Ortega, E., 2016. El uso de la cal en la construcción durante la Prehistoria reciente: Nuevas aportaciones para el Levante de la Península Ibérica. Arqueología de la Arquitectura 13, 1–18. https://doi.org/10.3989/arq.arqt.2016.005.

Kirboga, S., Oner, M., 2013. Effect of the experimental parameters on calcium carbonate precipitation. Chemical Engineering Transactions 32, 2119–2124. https://doi.org/10.3303/CET1332354.

Lecomte-Nana, G.L., Bonnet, J.P., Blanchart, P., 2011. Investigation of the sintering mechanisms of kaolin–muscovite. Applied Clay Science 51 (4), 445–451. https://doi.org/10.1016/j.clay.2011.01.007.

Levytskyi, V., Sobolevskyi, R., Zawieska, D., Markiewicz, J., 2017. The accuracy of determination of natural stone cracks parameters based on terrestrial laser scanning and dense image matching data. In: 17th International Multidisciplinary Scientific Conference SGEM2017. International Multidisciplinary Scientific Geoconference, pp. 255–262. https://doi.org/10.5593/sgem2017/23/S10.031.

Linares-Catela, J.A., Vera-Rodríguez, J.C., 2023. Small Houses of the Dead: A Model of Collective Funerary Activity in the Chalcolithic Tombs of Southwestern Iberia. La Orden-Seminario Site (Huelva, Spain). Open Archaeology 9, 20220294. https://doi.org/10.1515/opar-2022-0294.

Linares-Catela, J.A., Donaire Romero, T., Mora Molina, C., Cáceres Puro, L.M., 2023. Choosing the site, getting the stones, building the dolmens: local sourcing of andesites at the El Pozuelo megalithic complex (Huelva, Spain). Archaeological and Anthropological Sciences 15, 101. https://doi.org/10.1007/s12520-023-01799-0.

Lull, V., et al., 2021. Emblems and spaces of power during the Argaric Bronze Age at La Almoloya, Murcia. Antiquity 1–20. https://doi.org/10.15184/aqy.2021.8.

Maravelaki, P.N., Theologitis, A., Budak Unaler, M., Kapridaki, C., Kapetanaki, K., Wright, J., 2021. Characterization of ancient mortars from minoan city of kommos in crete. Heritage 4 (4), 3908–3918. https://doi.org/10.3390/heritage4040214.

Márquez-Romero, J.E., Jiménez-Jaimez, V., 2013. Monumental ditched enclosures in southern Iberia (fourth–third millennia BC). Antiquty 87 (336), 447–460.

Mendelovici, E., 1997. Comparative study of the effects of thermal and mechanical treatments on the structures of clay minerals. Journal of Thermal Analysis and Calorimetry 49 (3), 1385–1397. Crete.

Munawaroh, F., Muharrami, L., Triwikantoro, K., Arifin, Z., 2019. Synthesis and characterization of precipitated $CaCO_3$ from ankerite prepared by bubbling method. In: KnE engineering: International conference on basic sciences and its applications, pp. 98–104. https://doi.org/10.18502/keg.v1i2.4435.

Nieto Gallo, Sánchez Meseguer, J., 1980. Excavaciones arqueológicas en España: El Cerro de la Encantada, Granátula de Calatrava (Ciudad Real). Ministerio de Cultura, Dirección General de Bellas Artes. In: Archivos y Bibliotecas, Subdirección General. de Arqueología, Madrid.

Pastor Quiles, M., 2017. La construcción con tierra en arqueología: Teoría, método, técnicas y aplicación. Publicaciones de la Universitat d'Alacant, Alicante.

Pastor Quiles, M., 2021. Procesos constructivos y edificación con tierra durante la Prehistoria reciente en las tierras meridionales valencianas. Serie de trabajos varios. Diputación de Valencia, Valencia, Spain.

Riquelme, A., Martínez-Martínez, J., Martín-Rojas, I., Sarro, R., Rabat, A., 2022. Control of natural fractures in historical quarries via 3D point cloud analysis. Engineering Geology 301, 106618. https://doi.org/10.1016/j.enggeo.2022.106618.

Rodríguez, R.M., 2018. Re-excavando Santa Trega (A Guarda, Pontevedra). Nuevos datos y conclusiones del Barrio Mergelina. Férvedes 9, 107–116.

Rodriguez, J.P., Soto, P.S., 1991. The influence of the dry grinding on the thermal behaviour of pyrophyllite. Journal of Thermal Analysis and Calorimetry 37 (7), 1401–1413.

Saikia, B.J., Parthasarathy, G., Sarmah, N.C., 2008. Fourier transform infrared spectroscopic estimation of crystallinity in SiO_2-based rocks. Bulletin of Materials Science 31, 775–779. https://doi.org/10.1007/s12034-008-0123-0.

Sánchez Meseguer, J.L., Galán Saulnier, C., 2001. Restos, huellas y evidencias. Complejos de Culto en el Cerro de La Encantada. In: Büchner, D. (Ed.), Studien in memoriam Wilhelm Schüle. Internationale archäologie-studia honoraria, vol. 11. Verlag Marie Leidorf, Rahden, pp. 379–417.

Sánchez Meseguer, J., Fernandez, A., Galán, C., Poyato, C., Romero, H., 1983. El Oficio y La Encantada: Dos ejemplos de culto en la Edad del Bronce en la Península Ibérica. In: XVI congreso nacional de arqueología. Zaragoza, pp. 383–396.

Sánchez Meseguer, J.L., Galán Saulnier, C., 2004. La Península Ibérica en el II milenio a. C.: Poblados y fortificaciones, el «Cerro de la Encantada». In: Humanidades, vol. 77. Ediciones de la Universidad de Castilla-La Mancha, Cuenca.

Sánchez Meseguer, Galán Saulnier, C., 2019. La cronología del Cerro de La Encantada: Estratigrafía, dataciones radiocarbónicas y paleoclimatología. Calatrava Estudios 1, 89–130.

Singh, M., Kumar, S.V., Waghmare, S.A., Sabale, P.D., 2016. Aragonite–vaterite–calcite: Polymorphs of $CaCO_3$ in 7th century CE lime plasters of alampur group of temples india. Construction and Building Materials 112, 386–397. https://doi.org/10.1016/j.conbuildmat.2016.02.186.

Smith, G.P.S., Gordon, K.C., Holroyd, S.E., 2013. Raman spectroscopic quantification of calcium carbonate in spiked milk powder samples. Vibrational Spectroscopy 67, 87–91. https://doi.org/10.1016/j.vibspec.2013.04.005.

Smykatz-Kloss, W., 1974. Differential thermal analysis: Application and results in mineralogy. Springer-Verlag, Berlin.

Tanbakouei, S., Michalski, J.R., 2023. Raman spectroscopy of clay standards as an analogue of martian clays. In: 54th lunar and planetary science conference 2023 (LPI contrib. No. 2806). Department of Earth Science, Hong Kong.

Toffolo, M.B., Regev, L., Dubernet, S., Lefrais, Y., Boaretto, E., 2019. FTIR-based crystallinity assessment of aragonite-calcite mixtures in archaeological lime binders altered by diagenesis. Minerals 9 (2), 121. https://doi.org/10.3390/min9020121.

Wilson, R., 2010. Minerals and rocks. Ventus Publishing ApS, Aarhus University, Denmark.

Winter-Livneh, R., Svoray, T., Gilead, I., 2013. Shape reproducibility and architectural symmetry during the chalcolithic period in the southern levant. Journal of Archaeological Science 40, 1340–1353. https://doi.org/10.1016/j.jas.2013.01.015.